AD-A123 364 STATE OF THE ART IN OCEAN-ATMOSPHERE INTERFACE MODELING 1/1
(U) NAVAL OCEAN SYSTEMS CENTER SAN DIEGO CA
J A NEUBERT AUG 82 NOSC/TR-809

UNCLASSIFIED F/G 8/3 NL

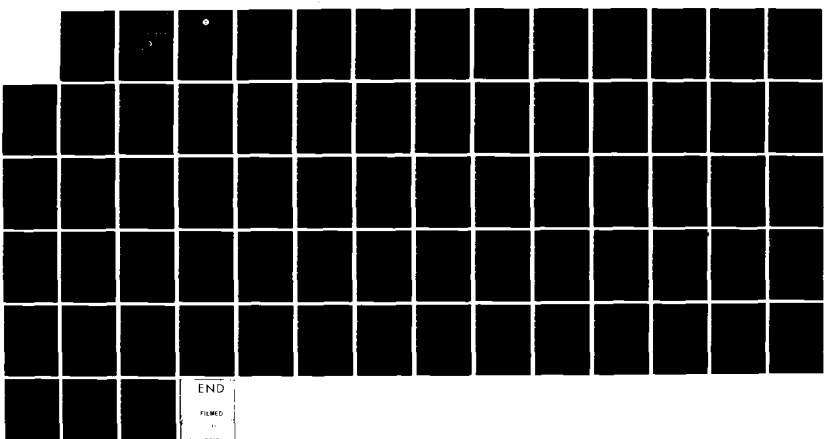

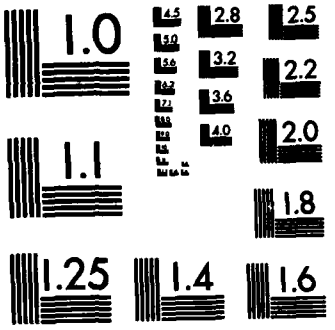

(12)

NOSC TR 809

NOSC TR 809

AD A123364

Technical Report 809

STATE OF THE ART IN OCEAN-ATMOSPHERE INTERFACE MODELING

JA Neubert

August 1982

Research report: May — August 1982

Prepared for
NOSC IRIED Program

Approved for public release; distribution unlimited.

DTIC FILE COPY

NAVAL OCEAN SYSTEMS CENTER
San Diego, California 92152

NAVAL OCEAN SYSTEMS CENTER, SAN DIEGO, CA 92152

AN ACTIVITY OF THE NAVAL MATERIAL COMMAND

JM PATTON, CAPT, USN
Commander

HL BLOOD
Technical Director

ADMINISTRATIVE INFORMATION

The work reported herein was funded by the NOSC Independent Research and Exploratory Development program and conducted over the period of May - August 1982.

Released by
JH Richter, Head
Ocean and Atmospheric
Sciences Division

Under authority of
JD Hightower, Head
Environmental Sciences
Department

UNCLASSIFIED

SECURITY CLASSIFICATION OF THIS PAGE *(When Data Entered)*

REPORT DOCUMENTATION PAGE		READ INSTRUCTIONS BEFORE COMPLETING FORM
1. REPORT NUMBER NOSC TR 809	2. GOVT ACCESSION NO. AD-A123 364	3. RECIPIENT'S CATALOG NUMBER
4. TITLE *(and Subtitle)* STATE OF THE ART IN OCEAN – ATMOSPHERE INTERFACE MODELING		5. TYPE OF REPORT & PERIOD COVERED Research report: May - August 1982
		6. PERFORMING ORG. REPORT NUMBER
7. AUTHOR(s) J.A. Neubert		8. CONTRACT OR GRANT NUMBER(s)
9. PERFORMING ORGANIZATION NAME AND ADDRESS Naval Ocean Systems Center, San Diego, CA 92152		10. PROGRAM ELEMENT, PROJECT, TASK AREA & WORK UNIT NUMBERS
11. CONTROLLING OFFICE NAME AND ADDRESS Naval Ocean Systems Center, San Diego, CA 92152		12. REPORT DATE August 1982
		13. NUMBER OF PAGES 68
14. MONITORING AGENCY NAME & ADDRESS *(if different from Controlling Office)*		15. SECURITY CLASS. *(of this report)* Unclassified
		15a. DECLASSIFICATION/DOWNGRADING SCHEDULE

16. DISTRIBUTION STATEMENT *(of this Report)*

Approved for public release; distribution unlimited

17. DISTRIBUTION STATEMENT *(of the abstract entered in Block 20, if different from Report)*

18. SUPPLEMENTARY NOTES

19. KEY WORDS *(Continue on reverse side if necessary and identify by block number)*

Ocean dynamics
Radar imaging
Surface reverberation
Gravity waves
Capillary waves

20. ABSTRACT *(Continue on reverse side if necessary and identify by block number)*

Two important naval modeling problems, acoustic torpedo surface reverberation in shallow water and remote radar sea surface imaging, are dependent on an understanding of sea surface gravity - capillary waves. To understand the state of the art in sea surface modeling, the fundamental mathematical relations are first reviewed and then applied to four phenomena that affect the spectra of short gravity - capillary waves. These four phenomena are wind velocity, surface current, swell, and internal waves. The most recent sea surface models for these phenomena are discussed and then a software modeling approach based upon the radiative transfer equation is suggested that would provide the requisite statistical parameters for treating the two naval modeling problems.

DD FORM 1 JAN 73 1473 EDITION OF 1 NOV 65 IS OBSOLETE
S/N 0102-LF-014-6601

UNCLASSIFIED

SECURITY CLASSIFICATION OF THIS PAGE *(When Data Entered)*

CONTENTS

NOTATION

A	Wave action density, where $A = E/\sigma$
c	phase speed for surface waves
c_g	group velocity of Eq (6) for surface waves
d_f	fetch
E	local energy density
$f(\theta)$	wind directional function of Eq (13)
$F(k)$	energy spectral density of Eq (12)
g	acceleration due to gravity
$\underline{k}$	wavenumber vector of magnitude k
m	slope, see Eq (98)
n	apparent or observed frequency of Eq (2)
$N(\underline{k})$	spectral action density, where $N(\underline{k}) = F(\underline{k})/\sigma$
S_i	source term of Eq (19), see also Eq (20) - (24)
$S_{\alpha\beta}$	radiation stress as found in Eq (7)
t	time
T	ratio of surface tension to water density
u_*	friction velocity
$X(\underline{k},n)$	displacement spectral density of Eq (10)
$\tilde{x}$	nondimensional fetch
$\underline{x}$	location vector
z	distance above the mean sea surface
α	see Eq (20)
β	see Eq (21)
γ	Phillips constant of Eq (14), (30)
$\lambda(\underline{k},\underline{k}')$	see Eq (22)

γ_f	attenuation coefficient in presence of dense slick
γ_v	attenuation coefficient for clean surface
$\varepsilon(\underline{k},\underline{k}')$	see Eq (23)
ζ	surface displacement about the mean surface
λ	wavelength, where $k = 2\pi/\lambda$
ν	kinetic viscosity
ρ	density
σ	intrinsic frequency whose $\underline{k}$ dependence gives the dispersion relation
$\phi(n)$	displacement frequency density of Eq (11a)
$\psi(\underline{k})$	displacement spectral density of Eq (11b)

I. INTRODUCTION

Two important naval system problems, acoustic torpedo surface reverberation in shallow water and remote radar sea surface imaging, have a common physical interface, ie, the sea surface. The proper and adequate modeling of the sea surface determines our ability to model and predict the behavior of homing torpedoes in shallow water and the imaging of remote radar sensors. Therefore, this report examines the state of the art in ocean–atmosphere interface modeling.

A survey of recent oceanographic literature showed that there are relatively few fundamental mathematical relations for modeling the sea surface. These relations are presented in Section II and applied in Section III. In addition, several useful theoretical results and empirical relations are included throughout this report. As shown throughout Section III, many models begin with the appropriate forms of the kinematical equation (Section II.A.) and the action conservation principle (Section II.B.). Sometimes the radiative stress equation (Section II.C) is used instead of the action conservation principle. A much older and less prolific relation, the Bernoulli equation, is discussed in one of its useful forms in Section II.D.

The waves found on the surface of the sea are almost always random in the sense that the detailed configuration of the sea surface varies in an irregular manner in both space and time. Therefore, only the various statistical measures of the surface motion can be regarded as significant observationally or predictable theoretically. Consequently, Sections II.E and II.F discuss various spectral relations (and their directional behavior) and concepts. Equation (18), the conservation of action spectral density, often proves to be a useful statistical relation for sea surface modeling purposes. However, the radiative transfer equation, Eq (19), promises to be the most

fruitful statistical relation for modeling the sea surface and is discussed in Section II.F.

The state of the art in practical ocean surface modeling is treated in Section III and represents the main results of this survey. The "mean JONSWAP spectrum" (Section III.B) is a well-accepted relation and provides a major empirical benchmark for many theoretical developments. This study was designed to treat the effect of four phenomena on the sea surface behavior. These four phenomena are wind velocity, surface current, swell, and internal waves. The directional behavior of the wind is discussed in Section II.E and the effects of its magnitude are shown in Section III.B. Four significant properties of a variable surface current are presented in Section III.C. These are (1) upwelling, (2) lateral spreading, (3) frequency-dependent attenuation, and (4) refraction of surface waves by a shear current. Section III.D discusses the interaction of swell and short gravity waves and gives some special consideration to imaging by a remote radar sensor. The most thoroughly developed and verified theory concerns the interaction of surface and internal waves. This is discussed in Section III.E. Finally, Section III.F considers wave attenuation.

In Section IV it is tentatively concluded that the state of the art in sea surface modeling is sufficiently developed to permit the two important naval system problems specified to be addressed. Therefore, Section IV proceeds to suggest a possible method of developing a software model for this purpose. The appendix examines imaging for remote radar sensing.

II. FUNDAMENTAL MATHEMATICAL RELATIONS

A. KINEMATICAL EQUATION

The kinematical equation (Ref 1) gives the kinematical conservation of the density of waves in the form

$$\frac{\partial \underline{k}}{\partial t} + \nabla n = 0 \tag{1}$$

as given by Ref 2 and 3, where $\underline{k}$ is the wavenumber vector and

$$n = \sigma + \underline{k} \cdot \underline{U} \tag{2}$$

is the apparent or observed frequency of waves passing a fixed point when the medium itself is moving with velocity $\underline{U}(\underline{x},t)$, which is a slowly varying function of position $\underline{x}$ and time t, and $\sigma = \sigma(\underline{k})$ is the intrinsic frequency whose $\underline{k}$ dependence represents the dispersion relation. The distribution of the local wavenumber $\underline{k}$ in space obeys

$$\nabla \times \underline{k} = 0. \tag{3}$$

In deep water

$$\sigma^2(k) = gk + Tk^3, \tag{4}$$

where g is the acceleration due to gravity, and T is the ratio of the surface tension to the water density (Ref 1, p 37-38). The first right-hand term in

---

1. O.M. Phillips, The Dynamics of the Upper Ocean, Cambridge University Press, 1977.

2. F. Unsell, "Steady wave patterns on a non-uniform fluid flow," J. Fluid Mech., 9, 1960, 333-346.

3. G.B. Whitham, "A note on group velocity," J. Fluid Mech., 9, 1960, 347-352.

Eq (4) represents gravity waves, while the second represents capillary waves; gravity waves dominate for wavelengths $\lambda > 10$ cm, where $k = 2\pi/\lambda$.

B. ACTION CONSERVATION PRINCIPLE

The action conservation principle [established by Bretherton and Garrett (Ref 4) and elaborated further by Bretherton (Ref 5); see also Ref 1, p 26-27] is

$$\frac{\partial A}{\partial t} + \nabla\cdot[(\underline{U} + \underline{c}_g)\cdot A] = 0, \tag{5}$$

where the wave action density $A = E/\sigma$, E is the local energy density, and

$$\underline{c}_g = \nabla_k \sigma(\underline{k}) \tag{6}$$

is the group velocity (Ref 1, p 25). Equation (5) is valid generally for nondissipative, short, small-amplitude waves in a moving medium. It states that the local rate of change of A is balanced by the convergence of the flux of A that flows relative to the moving medium with velocity $\underline{c}_g$. It can be shown that the phase speed c for a surface gravity wave obeys $c_g = \frac{1}{2}c$.

C. THE RADIATION STRESS EQUATION

If the fluctuating motion consists entirely of a wave train in which the energy dissipation is negligible, the energy balance is given by

---

4. F.P. Bretherton and C.J.R. Garrett, "Wavetrains in inhomogeneous moving media," Proc. Roy. Soc., A, 302, 1969, 529.

5. F.P. Bretherton, "The general linearized theory of wave propagation," in Mathematical Problems in the Geophysical Sciences, vol. 1, 61-102, Amer. Math. Soc., Providence, RI, 1971.

$$\frac{\partial E}{\partial t} + \frac{\partial}{\partial x_\alpha}\{E[U_\alpha + (c_g)_\alpha]\} + S_{\alpha\beta}\frac{\partial U_\beta}{\partial x_\alpha} = 0 \qquad (7)$$

(Ref 1, p 63-68, and Ref 6-8), where $\alpha,\beta = 1,2$ and the radiation stress $S_{\alpha\beta}$ represents the excess momentum flux associated with the wave motion alone. Phillips (Ref 1, p 68) shows that $S_{\alpha\beta} = S = \frac{1}{2}E$ in deep water.

D. THE BERNOULLI EQUATION

Starting with the momentum equation in the form

$$\frac{\partial \underline{u}}{\partial t} + \underline{\omega} \times \underline{u} + \nabla(p/\rho + \tfrac{1}{2}u^2 + gz) = \nu\nabla^2\underline{u} \qquad (8)$$

where p is the pressure, ρ is the density, ν is the kinetic viscosity, z is distance above the mean sea surface, $\underline{\omega} = \nabla \times \underline{u}$ is the vorticity, and expressing the particle velocity $\underline{u}$ in terms of the velocity potential ϕ or $\underline{u} = \nabla\phi$ gives (Ref 1, p 19-20) the Bernoulli equation for irrotational (or potential) flow with $\underline{\omega} = 0$ and $\nu = 0$

$$\frac{p}{\rho} + \frac{\partial\phi}{\partial t} + \tfrac{1}{2}u^2 + gz = f(t), \qquad (9)$$

where f(t) is an arbitrary function of time determined by the pressures imposed at the boundaries of motion.

---

6. M.S. Longuet-Higgins and R.W. Stewart, "Changes in the form of short gravity waves on long waves in tidal currents," J. Fluid Mech., 8, 1960, 565-583.

7. M.S. Longuet-Higgins and R.W. Stewart, "The changes in amplitude of short gravity waves on steady non-uniform currents," J. Fluid Mech., 10, 1961, 529-549.

8. G.B. Whitham, "Mass momentum and energy flux in water waves," J. Fluid Mech., 12, 1962, 135-147.

E. SOME SPECTRAL AND DIRECTIONAL RELATIONS

The mean square surface displacement is represented spectrally by

$$\overline{\zeta^2} = \int X(\underline{k},n)d\underline{k}dn \tag{10}$$

$$= \int_0^\infty \phi(n)dn = \int \psi(\underline{k})d\underline{k} \tag{11}$$

so that

$$E = \int F(\underline{k})d\underline{k} \tag{12}$$

$$= \rho g\overline{\zeta^2} = \rho g \int \psi(\underline{k})d\underline{k}.$$

From the directional material in Barnett and Kenyon (Ref 9, p 688-689, 713-714) and the "saturation range" material in Phillips (Ref 1, p 102-104, 140-149), the following useful relations can be obtained. Waves leaving a storm area can have a broad, say ±45°, directional distribution relative to the mean wind direction. Represent the directional spectrum $\phi_1(n,\theta)$ by

$$\phi_1(n,\theta) = \phi(n)f(\theta) \ , \tag{13}$$

where $\theta = 0°$ in the mean wind direction. For the saturation range Phillips (Ref 1, p 102-104, 149) gives

$$\phi(n) = \gamma g^2 n^{-5} \ , \ n_o << n << 2g/u_* \ , \tag{14}$$

where n_o is the spectrum peak apparent frequency, u_* is the friction velocity, and γ is a "constant" whose dimensionless fetch dependence is given by Eq (30) and

---

9. T.P. Barnett and K.E. Kenyon, "Recent advances in the study of wind waves," Rep. Prog. Phys., 38, 1975, 667-729.

$$\psi(\underline{k}) = Dk^{-4}f(\theta),\ k_o << k << 2g/u_*^2\ , \tag{15}$$

where k_o is the spectrum peak wavenumber magnitude, θ specifies the direction of $\underline{k}$ relative to the mean wind velocity, and $D \sim \frac{1}{2}\gamma$ (Ref 1, p 148-150). For an extension of Eq (14) to higher frequencies see Ref 10. For a critique of Eq (14) see Ref 11.

The distribution of wave energy in $\underline{k}$-space for a fully aroused sea was first estimated with some accuracy during the SWOP project (Ref 9, Section 4.2) by Cote, et al (Ref 12). The rough sea under the action of a steady wind gave

$$f(\theta) = 1 + a_1 e^{-b}\cos\theta + a_2 e^{-b}\cos 4\theta\ , \tag{16}$$

where the a_i are constants and $b = \frac{1}{2}(\sigma U/g)^4$. Basically this equation says that the waves are distributed as $\cos^2\theta$ near the spectral peak, with the beamwidth broadening at higher frequencies. A substantial advance in estimating $f(\theta)$ was made by Longuet-Higgins et al (Ref 13) and Cartwright and Smith (Ref 14):

$$f(\theta) = \cos^s\left(\frac{\theta}{2}\right),\ -\pi \leq \theta \leq \pi \text{ and } s = s(n). \tag{17}$$

---

10. H. Mitsuyasu, "Measurement of the high-frequency spectrum of ocean surface waves," J. Phys. Ocean., 7, 1977, 882-891.

11. S.A. Kitaigorodskii, "The statistical characteristics of wind-generated short gravity waves," in Spaceborne Synthetic Aperture Radar for Oceanography, R.C. Beal, et al., eds., The Johns Hopkins University Press, 1981.

12. C.S. Cote, et al., Meteorological Papers, 2(6), W.J. Pierson, Jr., ed., 1960.

13. M.S. Longuet-Higgins, D.E. Cartwright, and N.D. Smith, Ocean Wave Spectra, Prentice-Hall, 1963, 111-136.

14. D.E. Cartwright and N.D. Smith, Buoy Technology, Marine Technology Society, Washington, D.C., 1964, 112-121.

The values of s ranged from 1 for high frequencies to 10 at low frequencies. Ewing (Ref 15) confirmed these results. Phillips (Ref 16) suggests $f(\theta) = \cos^2\theta$ or $\cos^4\theta$ as a rough rule of thumb.

A further useful spectral equation is

$$\frac{\partial}{\partial t}N(\underline{k}) + (\underline{c}_g + \underline{U})\cdot\nabla N(\underline{k}) = 0, \tag{18}$$

where the spectral energy density is related to the spectral action density by $N(\underline{k}) = F(\underline{k})/\sigma$ (see Ref 1, p 181). Equation (18) expresses the conservation of action spectral density $N(\underline{k},\underline{x},t)$ of short waves.

F. THE RADIATIVE TRANSFER EQUATION

The radiative transfer equation, Eq (19), describes the energy balance of the wind wave field in terms of the energy spectrum $F(\underline{k})$ of surface gravity waves. This equation, which summarizes all the various physical processes S_i which can change the wave energy, is given by

$$\frac{dF}{dt} \equiv \frac{\partial F}{\partial t} + \frac{\partial x_i}{\partial t}\frac{\partial F}{\partial x_i} + \frac{\partial k_i}{\partial t}\frac{\partial F}{\partial k_i} = \sum_{i=1}^{n} S_i \ , \tag{19}$$

where the spectrum $F(\underline{k},\underline{x},t)$ is locally a function of $\underline{k}$ but is allowed to vary slowly as a function of $\underline{x}$ and t. The characteristic equations are

$$\frac{\partial x_i}{\partial t} = \frac{\partial \sigma}{\partial k_i} = c_{gi} \tag{6a}$$

---

15. J.A. Ewing, J. Marine Res., 27, 1969, 163-171.

16. O.M. Phillips, "The structure of short gravity waves on the ocean surface," in Spaceborne Synthetic Aperture Radar for Oceanography, R.C. Beal, et al, eds., The Johns Hopkins University Press, 1981.

and

$$\frac{\partial k_i}{\partial t} = - \frac{\partial n}{\partial x_i} \tag{1a}$$

and are equivalent to Hamilton's equation for a particle. Barnett and Kenyon (Ref 9, p 678-684, 698-704, 718-722) survey the state of the art of applying Eq (19). Hughes (Ref 17) applies Eq (19) to the interaction of internal waves and surface wind waves.

Hasselmann (Ref 18) and Barnett and Kenyon (Ref 9, p 678-682) give some forms for the source functions S_i, namely

$$S_1 = \alpha \tag{20}$$

$$S_2 = \beta F(\underline{k}) \tag{21}$$

$$S_3 = F(\underline{k}) \int \gamma(\underline{k},\underline{k}')F(\underline{k}')d\underline{k}' \tag{22}$$

$$S_4 = -\delta F(\underline{k}) + \int \varepsilon(\underline{k},\underline{k}')F(\underline{k}')d\underline{k}' \tag{23}$$

$$S_5 = \int [T_1 F(\underline{k}')F(\underline{k}-\underline{k}'-\underline{k}'') - T_2 F(\underline{k})F(\underline{k}')F(\underline{k}'')]d\underline{k}'d\underline{k}'' \ . \tag{24}$$

The Phillips linear growth function S_1 represents the constant energy transfer to the wave field through turbulent atmospheric pressure fluctuations. The Miles exponential growth function S_2 represents the increasing transfer of energy to the wave field due to an instability in the coupling between the wave field and the mean boundary layer flow in air. The term S_3 is a nonlinear correction to S_2. The term S_4 represents the energy transfer due to the interaction between waves and turbulence in the atmosphere. The term S_5

---

17. B.A. Hughes, "The effect of internal waves on surface wind waves. 2: Theoretical analysis," J. Geophys. Res., 83, 1978, 455-465.

18. H. Hasselmann, Basic Developments in Fluid Dynamics, Vol. 2, M. Holt, ed., Academic Press, 1968, 117-182.

represents the energy transfer among the various wavenumber components due to weak nonlinear wave-wave interactions; S_5 is further treated in Ref 9, p 682-684, and is discussed in Ref 1, p 135-140, where the equation

$$\frac{\partial N_1}{\partial t} = 4\pi k_o^6 \int [(N_1 + N_2)N_3N_4 - (N_3 + N_4)N_1N_2]$$

$$\cdot \delta(\sigma_1 + \sigma_2 - \sigma_3 - \sigma_4)\delta(\underline{k}_1 + \underline{k}_2 - \underline{k}_3 - \underline{k}_4)d\underline{k}_2 d\underline{k}_3 d\underline{k}_4 , \qquad (25)$$

$N_i = N(\underline{k}_i)$, is found to be valid in the neighborhood of the spectral peak at $k = k_o$ (Ref 19). See also Fig 4 of Ref 9, where the "overshoot effect" in the spectral density development is shown.

Recent results on prediction models based on the radiative transfer equation are discussed in Ref 9, p 721-722. Barnett (Ref 20, 21) used finite-difference methods to solve the radiative transfer equation over the entire North Atlantic under the following assumptions:

$$\frac{\partial F}{\partial t} + \dot{x}_i \frac{\partial F}{\partial x_i} = S_1 + S_2 \pm S_5 - S_6 , \qquad (26)$$

where S_1 is a version of Phillips' resonance theory modified by the observations of Section 5.1 of Ref 9; S_2 is an exponential growth term based entirely on the observations described in Section 5.1 of Ref 9; S_5 represents computer-simplified parameterizations of the wave-wave interactions; and S_6 is a representation of wave breaking (limiting growth) based on the equilibrium ideas of Phillips as described in Section 5.5 of Ref 9. No assumption of a

---

19. M.S. Longuet-Higgins, "On the nonlinear transfer of energy in the peak of a gravity-wave spectrum: a simplified model," Proc. Roy. Soc., A, 437, 1976, 311-328.

20. T.P. Barnett, "On the generation, description, and prediction of ocean wind waves," Ph.D. dissertation, University of California, San Diego, 1966.

21. T.P. Barnett, "On the generation, description, and prediction of ocean wind waves," J. Geophys. Res., 73, 1968, 513-529.

fully developed spectrum was made. The same approach has been followed by Ewing (Ref 22). His formulation utilized a more accurate parametric version due to Cartwright of the term S_5 and a higher-order finite-difference approximation for the advective term of Eq (19). Ewing's comparisons were made against the two-dimensional spectrum, the first such verifications attempted. The results gave, in Ewing's words, "adequate estimates of the significant height and one-dimensional wave spectrum. The standard deviation of all the computed estimates of $H_{1/3}$ [the significant wave (the mean of the highest third of all waves present)] compared to measurements is about 0.6 m. Reliable estimates of the two-dimensional wave spectrum were only achieved in a limited region at the high-frequency end of the spectrum." This later discrepancy was attributed to inadequate specification of the wind field.

---

22. J.A. Ewing, "A numerical wave prediction for the North Atlantic Ocean," Deutsche Hydrog. Z., 24, 1971, 241-261.

III. STATE OF THE ART IN PRACTICAL OCEAN SURFACE MODELING

A. INTRODUCTION

An important empirical relation is the "mean JONSWAP spectrum," Eq (27). This is discussed in Section III.B along with some other useful empirical relations. Using Eq (27) allows the wind speed magnitude to be considered; the directional behavior of the wind is addressed in Section II.E, especially Eq (17). Surface waves in a variable current are discussed in Section III.C, where direction and energy density relations are given for four situations: (1) upwelling, (2) lateral spreading, (3) frequency-dependent attenuation, and (4) refraction of surface waves by a current shear. Section III.D treats the interaction of swell and short gravity waves. Equation (73) represents a key result for imaging by a remote radar sensor. The interaction of surface and internal waves, Section III.E, is our best-understood phenomenon. Particular emphasis is given to the approaches of Phillips (Ref 1, p 78-81, and Ref 23), Ko (Ref 24), and Hughes (Ref 17). Finally wave attenuation is addressed in Section III.F.

Weak wave-wave interactions will not be discussed further since they are covered thoroughly in Ref 1, p 27-32, 81, 135-140, and Ref 9, p 682-684. On the other hand, long wave–short wave interaction is still a controversial subject. Garrett and Smith (Ref 25) update the survey material contained in Ref 9, p 690-691, and conclude that the long waves can grow if short wave

---

23. O.M. Phillips, "On the interactions between internal and surface waves," Phys. Atmos. and Oceans, 9, 1973, 954-961.

24. J.E. Lewis, B.M. Lake, and D.R.S. Ko, "On the interaction of internal waves and surface gravity waves," J. Fluid Mech., 63(4), 1974, 773-800.

25. C. Garrett and J. Smith, "On the interaction between long and short surface waves," J. Phys. Oceanogr., 6, 1976, 925-930.

generation is correlated with the long wave orbital velocity. Reference 26 is very instructive and contains some tools from which a model can be built. References 27 and 28 give some experimental results; the latter paper uses swells as the long waves. Valenzuela and Wright (Ref 29) use the radiative transfer equation, developed for gravity-capillary waves, but their work is too theoretical for easy model development.

B. THE MEAN JONSWAP SPECTRUM

Phillips (Ref 1, p 139-140) and Barnett and Kenyon (Ref 9, p 715-717) reviewed the "mean JONSWAP spectrum." Fox (Ref 30) found for the mean JONSWAP spectrum an empirical fit to results from the Joint North Sea Wave Project (Ref 31) as follows:

$$\phi_1(n) = \gamma g^2 n^{-5} \exp\left[-\frac{5}{4}\left(\frac{n}{n_o}\right)^{-4}\right]\left(\gamma_a\right)^{h_a} , \qquad (27)$$

---

26. O.M. Phillips, "The dispersion of short wavelets in the presence of a dominant long wave," J. Fluid Mech., 107, 1981, 465-485.

27. O.H. Shemdin, "Modulation of centimetric waves by long gravity waves: Progress report on field and laboratory results," NATO Conference on Turbulent Fluxes Through the Sea Surface, Wave Dynamics and Prediction, A. Farve and K. Hasselmann, eds., NATO Conference Series V, vol. 1, 1977.

28. E.D. Graves and O.H. Shemdin, "An investigation of the modulation of capillary and short gravity waves in the open ocean," J. Geophys. Res., 85(C9), 1980, 5019-5024.

29. G.R. Valenzuela and J.W. Wright, "Modulation of short gravity-capillary waves by longer-scale periodic flows--a higher-order theory," Radio Science, 14(6), 1979, 1099-1110.

30. M.J.H. Fox, "On the nonlinear transfer of energy in the peak of a gravity-wave spectrum--I," Proc. Roy. Soc., A 348, 1976, 467-483.

31. K. Hasselmann, et al, "Measurements of wind wave growth and swell decay during the Joint North Sea Wave Project (JONSWAP)," Herausgegeben von Deutsche Hydrograph. Institut, Reihe A, 12, 1973.

where

$$h_a = \exp\left[-\frac{(n - n_o)^2}{2m^2 n_o^2}\right], \tag{28}$$

$m = m_a$ for $n \leq n_o$ and $m = m_b$ for $n > n_o$. This form contains five parameters: γ, γ_a, m_a, m_b and the frequency of the spectral peak n_o. Note that Eq (27) is an extension of Eq (14) to all frequencies. For the mean JONSWAP spectrum, $\gamma_a = 3.3$, $m_a = 0.07$ and $m_b = 0.9$. Figure 17 of Ref 9 gives γ and n_o as a function of the nondimensional fetch

$$\tilde{x} = d_f g/U^2, \tag{29}$$

where d_f is the fetch and the U is the wind speed in the forms

$$\gamma = \gamma(\tilde{x}) = 0.076\ \tilde{x}^{-2.2} \tag{30}$$

(see also Table 4.1 of Ref 1) and

$$n_o = n_o(\tilde{x}) = 2\pi \cdot 3.5\ \tilde{x}^{-0.33}\ . \tag{31}$$

In Ref 1, p 148, 161, the following useful relations are found:

$$n_o \simeq 2.2(g^3/u_*^2 d_f)^{\frac{1}{3}} \tag{32}$$

$$U(z) = \frac{u_*}{\kappa_o} \log\left(\frac{z}{n_o}\right) - \frac{Bu_*}{2\kappa_o} f(k_o z)\ , \tag{33}$$

where

$$f(k_o z) = (k_o z)^2 \int_1^\infty t^{-3}\, e^{-2k_o z t}\, dt\ , \tag{34}$$

$$n_o \simeq 1.1 \cdot 10^{-2}\ u_*^2/g\ , \tag{35}$$

$\kappa_o \simeq 0.42$ is Kármán's constant, $B \simeq 2 \cdot 10^{-3}$ and k_o is the wavenumber spectral peak.

C. WAVES ON A VARIABLE CURRENT

Waves on a variable current are treated in Ref 1, p 74-78, and Ref 16. When a wave train encounters a current in which the surface velocity varies, the excess momentum flux results in an interchange of energy between waves and current. Suppose that the current strength varies along the direction of flow so that $U = U(x)$ in Eq (2); a situation like this may be encountered at an estuarine outflow with waves incident from the open sea. If α represents the angle between the local wavenumber and the current in the x-direction, then Eq (1) and (2) for a steady wave train in deep water give

$$n = \sigma + kU \cos \alpha = \text{const.} = \sigma_o = g/c_o = (gk_o)^{\frac{1}{2}} , \tag{36}$$

where σ_o is the wave intrinsic frequency in the open sea, where $U = 0$. Also Eq (3) gives

$$k \sin \alpha = k_o \sin \alpha_o = \text{const.} \tag{37}$$

The wavenumber component in the y-direction is conserved. From these two expressions

$$(gk)^{\frac{1}{2}} + U[k^2 - k_o^2 \sin^2 \alpha_o]^{\frac{1}{2}} = \sigma_o . \tag{38}$$

With a current in the same direction as that in which the waves are traveling, $U > 0$ and the wavenumber k is reduced, the wavelength increases, and the wave paths are turned away from the current. In an adverse current, on the other hand, $U < 0$, and the waves turn into the current as they shorten. Their group velocity decreases and they become less able to propagate against the current. If the strength of the latter is sufficient, an interesting phenomenon of blockage occurs. The algebra is simplest when $\alpha = 0$ and the

waves are running directly into the current. Equation (38) then becomes a simple quadratic equation in $k^{\frac{1}{2}}$, or equivalently in the local phase velocity c $= (g/k)^{\frac{1}{2}}$, with the solution

$$\frac{c}{c_o} = \frac{1}{2} + \frac{1}{2}\left(1 + \frac{4U}{c_o}\right)^{\frac{1}{2}} \tag{39}$$

which has a critical point at $U = -\frac{1}{2}c = -c_g$, where energy can no longer be propagated against the current. This is a kinematical limit; the waves break before this point. In summary, for waves in the presence of an adverse current, the waves turn toward the stream. Their local wavelength decreases and the energy density increases as the waves are pushed toward saturation and possible blockage. In a favorable current they turn away from the current, the local wavelength increases, the energy density is reduced, and the waves become less saturated.

Equation (5) gives

$$E(U + \tfrac{1}{2}c)c = \text{const.} = \tfrac{1}{2}E_o c_o^2 \tag{40}$$

which was originally derived by Longuet-Higgins and Stewart (Ref 7) from Eq (7). In the absence of wave breaking, the local amplitude is given by (see Fig 3.6 of Ref 1)

$$\frac{a}{a_o} = \frac{c_o}{[c(c + 2U)]^{\frac{1}{2}}} = \left(\frac{E}{E_o}\right)^{\frac{1}{2}} . \tag{41}$$

When the convergence of the current is balanced, not by upwelling as above, but by lateral spreading,

$$\frac{\partial U}{\partial x} + \frac{\partial V}{\partial y} = 0 . \tag{42}$$

If the flow is symmetrical about the line y = const., then on this line

$$\frac{a}{a_o} = \left[\frac{c}{c + 2U}\right]^{\frac{1}{2}} . \tag{43}$$

Now assume Eq (16) applies. Suppose that the wind-generated waves are unidirectional and move in direct opposition to the local current. In a frequency band $d\sigma$ in still water, the wave energy is initially, via Eq (16),

$$\phi_o(\sigma)d\sigma = \gamma g^2\sigma^{-5}d\sigma . \tag{44}$$

At the point where the adverse current is the greatest, ($U = -U_m$), the frequency of this band is σ' and the wave energy is

$$\phi_1(\sigma) = \gamma g^2(\sigma')^{-5} . \tag{45}$$

As the current decreases to zero, the frequency of the band returns to σ and the wave energy is reduced by the expansion to $\phi_2(\sigma)d\sigma$. In this part of the motion, no energy is lost by wave breaking. Equation (40) gives

$$\phi_1(\sigma')d\sigma'(c' - 2U_m)c' = \phi_2(\sigma)d\sigma c^2 , \quad c' = g/\sigma', \quad c = g/\sigma . \tag{46}$$

Equation (38) with $\alpha = 0$ gives

$$\sigma = \sigma' - k'U_m = \sigma' - \sigma'^2U_m/g . \tag{47}$$

Hence

$$\phi_2(\sigma) = \gamma g^2\sigma^2(\sigma')^{-7} \tag{48}$$

and

$$\frac{\phi_2(\sigma)}{\phi_o(\sigma)} = \left(\frac{\sigma}{\sigma'}\right)^7 , \tag{49}$$

where

$$\frac{\sigma}{\sigma'} = \tfrac{1}{2}\left[1 + \left(1 - \frac{4U_m\sigma}{g}\right)^{\frac{1}{2}}\right] . \tag{50}$$

A slowly varying current case is treated in Ref 32.

Refraction of surface waves by shear is probably encountered more frequently in the ocean than the situation just described, particularly at oceanic fronts, where a contrast in surface temperature is necessarily accompanied by shear. Since surface waves are dispersive, refraction effects by currents are stronger than they are in nondispersive waves.

The wave patterns can be analyzed in a manner similar to that given above. If α represents the angle between the local wavenumber and the current and $U = U(y)$ represents the shearing surface current, Eq (1) and (2) give

$$\sigma + kU \cos \alpha = \sigma_o \tag{51}$$

but now $\underline{k} = \underline{k}(y)$ in Eq (3) gives

$$k \cos \alpha = k_o \cos \alpha_o = \text{const.} \tag{52}$$

From these expressions and the dispersion relation $\sigma = (gk)^{\frac{1}{2}}$, it follows that

$$\cos \alpha = \frac{gk_o \cos \alpha_o}{(\sigma_o - k_o U \cos \alpha_o)^2} \quad , \tag{53}$$

which is necessarily less than or equal to unity. If $\cos \alpha_o < 0$ and the waves approaching the current are opposed to it, they will be turned toward the normal. If $\cos \alpha_o > 0$, however, they are turned away, the effect being augmented beyond simple convection by the dispersive nature of the waves. Just as the local wavelength increases as a result of the stretching, so does the wave velocity. The maximum penetration of the waves into the current system is reached when $\alpha = 0$ and

---

32. D. Holliday, "Nonlinear gravity-capillary surface waves in a slowly varying current," J. Fluid Mech., 57(4), 1973, 797-802.

$$\frac{U}{c_o} = \frac{1 - (\cos \alpha_o)^{\frac{1}{2}}}{\cos \alpha_o} \quad . \tag{54}$$

The waves are then refracted back by the stream. When the initial angle of incidence between the waves and the current, α_o, is relatively small, the stream current needed to turn back the waves is also small, approximately $\alpha_o^2 c_o/4$, where α_o is measured in radians.

The distribution of wave energy density can be found from Eq (5). Since U = U(y), the flux of wave action normal to the current is independent of y:

$$(Ec_g/\sigma) \sin \alpha = \text{const.} \tag{55}$$

or, since $c_g = g/2\sigma$,

$$E \sin \alpha \propto \sigma^2 = [\sigma_o - U(y)k_o \cos \alpha_o]^2 \tag{56}$$

from Eq (51) and (52), with again a theoretical singularity in E at $\alpha = 0$ when Eq (54) is satisfied. Note that from Eq (53) and (56)

$$E \sin 2\alpha = \text{const.} \tag{57}$$

Waves refracted toward the normal to the current are reduced in energy density; in those refracted away from the normal, the local energy density is augmented. The same is true for the mean square slope, which is proportional to Ek^2:

$$\frac{Ek^2}{E_o k_o^2} = \frac{\sin 2\alpha_o + \frac{1}{2} \sin 4\alpha_o}{\sin 2\alpha + \frac{1}{2} \sin 4\alpha} \quad , \tag{58}$$

so that wave trains refracted back from the current are driven toward local saturation as the turning line $\alpha = 0$ is approached.

How may these variations be reflected in the SAR (synthetic aperture radar)* imagery, in which a given wavenumber on the surface is sampled,

---

*See appendix.

not a given wave train? If the instrument is looking directly across the current, $\alpha = \alpha_o = \pi/2$; the wavenumber and energy density are unchanged and there is little reason to expect that the stream will be detected at all. If the current U has a positive component along the direction of observation, as U increases with range, for example, it will sample waves that are closer to local saturation; but beyond the line of maximum wave penetration, the return signal would be expected to be much less. If U has a negative component along the direction of observation, outwardly travelling waves will be refracted toward the normal; their mean square slope decreases and they become less saturated, giving a reduced signal intensity, provided the wind regeneration distance is large enough. The behavior of approaching wave trains can be inferred similarly.

D. INTERACTION OF SWELL AND SHORT GRAVITY WAVES

We turn to Phillips (Ref 16) for a discussion of the modification of short waves by swell. The short wave components are convected and distorted by longer waves or swell. Short wave energy and amplitude are in fact concentrated near the crests of the long waves and somewhat depleted in the troughs. In an actively generated wind-wave field, the short components may then be saturated only locally, near the long wave crests, and somewhat undersaturated elsewhere. The long waves propagate faster than the short waves so that a given group of short waves, being overtaken by a swell crest, may become saturated with local sporadic breaking, then--as the crest moves past--become unsaturated as it slips into the trough. It continues, however, to receive energy from the wind; and, if the input is sufficient, it is ready

again for more occasional wave breaking just before and at the next crest of the swell. This local saturation at the crests of the swell thus produces a modulation in the return signal of a SAR that enables the long wave pattern to be discerned if its wavelength is greater than about twice the discrimination distance. This effect is enhanced somewhat by a stationary wave effect when short waves, whose wavelength varies with respect to the phase of the swell, are viewed with the fixed radar wavelength signal. The steepness of the spectrum of Eq (15) provides further enhancement. Field studies by Evans and Shemdin (Ref 28) have demonstrated this modulation in radar return signals and associated them clearly with variations in short wave structure produced by longer waves.

The modulation of short wave structure by swell was first analyzed correctly by Longuet-Higgins and Stewart (Ref 6), but their analysis was limited to conditions in which the swell amplitude is less than the short wave wavelength. Numerical calculations that are free of this restriction were performed by Longuet-Higgins (Ref 33), and if (as is the situation of interest here) the ratio of long to short wavelength is large, simple asymptotic methods can be used. The details of this are given by Phillips (Ref 26).

These analyses were concerned with individual wave trains. For the present purpose they must be extended: (a) to allow for an arbitrary direction of propagation of the short waves relative to the swell, (b) to express the results of the interaction in terms of the local short wave spectral density, and (c) to determine the magnitude of the modulations in short wave spectral density of a fixed wave number on the surface, not on a given energy path along which the wavenumber varies.

---

33. M.S. Longuet-Higgins, "The instabilities of gravity waves of finite amplitude in deep water, Part I: Superharmonics," Proc. Roy. Soc. A 360, 1978, 471-488.

The geometry is illustrated in Fig 1. Axes x and y are chosen in the direction of swell propagation and along the crests, respectively; ϕ is the angle between the direction of observation and the direction of swell propagation, and θ_w is the direction of the local wind relative to the viewing direction. In a frame of reference moving with the swell, let its surface displacement be $\zeta_s = A \cos Kx = A \cos \chi$. The short, locally generated wind waves are riding over the swell; the local wavelength of a wave train and its direction of propagation vary as a result of the variable orbital velocities and vertical accelerations produced by the swell. In this frame of reference, the near-surface velocity is

$$U = -C(1 - AK \cos \chi) \tag{59}$$

in the positive x-direction, where C and AK represent the phase speed and slope of the swell, respectively. The effective gravitational acceleration experienced by the short waves is

$$g' = g(1 - AK \cos \chi) \tag{60}$$

as shown in Ref 26.

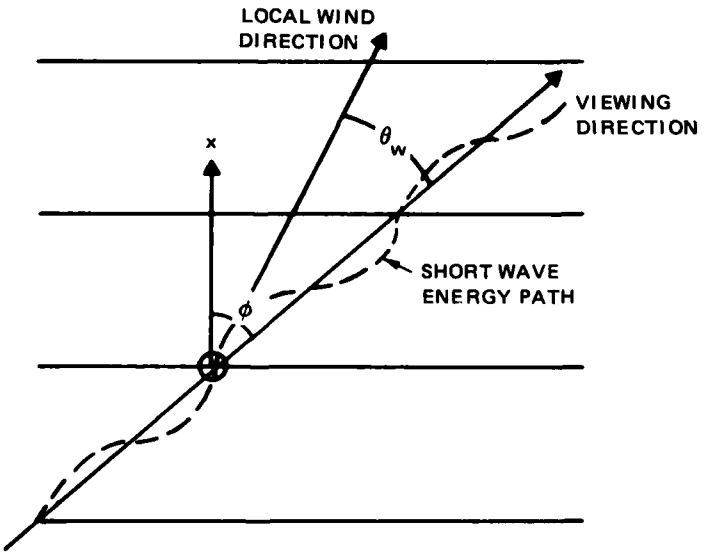

Figure 1. Short wave trajectories riding on a swell.

In the frame of reference moving with the swell $\partial/\partial t = \partial/\partial y = 0$, so Eq (1) and (3) reduce to

$$\frac{\partial}{\partial x}[\sigma - k_1 C(1 - AK \cos \chi)] = 0 \tag{61}$$

and

$$\frac{\partial k}{\partial x}^2 = 0 \ , \tag{62}$$

respectively, where $\underline{k} = (k_1, k_2)$ in the x- and y-directions, respectively. Equations (4) and (60) render

$$\sigma^2 = g'k \ , \tag{63}$$

and it follows that

$$2\sigma\frac{\partial\sigma}{\partial k} = gkK(AK) \sin \chi + g' \cos \phi \frac{\partial k}{\partial x}^{-1} \ . \tag{64}$$

Equation (61) gives

$$\frac{\partial k}{\partial x}^{-1} = -kK(AK)G(C,c,\phi) \sin \chi \ , \tag{65}$$

where

$$G(C,c,\phi) = \frac{C \cos \phi - c/2}{C - \frac{1}{2}c \cos \phi} \ , \tag{66}$$

to the lowest order in AK. The modulations in wavenumber are strongest when $\phi = 0$ and disappear when $\cos \phi = c/2C << 1$, that is, when the short waves are running almost along the crests of the swell. It is interesting to note that short waves propagating exacting along the swell crests are deformed somewhat since the effective gravitational acceleration experienced by the short waves is smaller there and the propagation speed is smaller than in the troughs.

Between long wave crests, when the short waves are unsaturated, the dynamics of the interaction are expressed most simply by Eq (18). For short gravity wavelengths of the order of 30 cm, energy input from the wind from one swell crest to the next can be ignored if, as is generally the case, T_w of Eq (67) is substantially larger than the swell period; T_w is the time scale over which the energy density decreases by a factor e in the absence of dissipative processes such as wave breaking and when $c > 10\ u_*$ or so, and is given by

$$T_w \sim 20c^2/\sigma u_*^2 \tag{67}$$

or

$$T_w \sim 3(c^2/u_*)^2 \quad \text{(wave periods)} \ . \tag{67}$$

In a frame of reference moving with the swell, the distribution of N(k) is steady so that

$$(\underline{c}_g + \underline{U})\cdot\nabla N(\underline{k}) = 0 \ . \tag{68}$$

Consequently $N(\underline{k})$ is constant along ray trajectories, though $\underline{k} = \underline{k}(\underline{x})$, and so if the local wind field is uniform, it is constant throughout. Thus, in particular,

$$\frac{dN}{dx} = 0 = \frac{\partial N}{\partial x} + \frac{\partial N}{\partial k_i}\frac{\partial k_i}{\partial x} \quad , \tag{69}$$

where $\partial N/\partial x$ expresses the variation at a fixed wavenumber $\underline{k}$ as sampled by the SAR. Furthermore, since $\partial k_2/\partial x = 0$,

$$\frac{\partial N}{\partial x} = -\frac{\partial N}{\partial k_1}\frac{\partial k_1}{\partial x}$$

$$= -\left[\cos(\phi - \theta_w)\frac{\partial N}{\partial k} + \sin(\phi - \theta_w)\frac{1}{k}\frac{\partial N}{\partial \theta_w}\right]\frac{\partial k_1}{\partial x} \tag{70}$$

in terms of the polar coordinates of Fig 1. The amplitude of the modulations in short wave action spectra at a fixed wavenumber is then

$$\delta N = -\left(\frac{\partial N}{\partial k_1}\right)\delta k_1$$

$$= -\left[\left(\frac{\partial N}{\partial k_1}\right)kG(C,c,\phi)\right](AK) \qquad (71)$$

from Eq (65) and is proportional to the swell slope AK.

Further progress is dependent on some knowledge of the $N(\underline{k})$. If, near the swell crests, the locally generated wind waves are close to saturation at the wavenumbers providing the backscattering, with local energy input from the wind being balanced largely by sporadic small-scale wave breaking, the spectral density of the short waves is given by Eq (15), where $f(\theta)$ is symmetrical about the wind direction. The corresponding action spectral density is

$$N(\underline{k}) = \psi(k)/\sigma = Df(\theta)g^{-\frac{1}{2}}k^{-9/2} , \qquad (72)$$

so that from Eq (65), (70), and (71), the amplitude of the modulations $\delta\psi$ in short wave spectral density at a fixed wavenumber referred to the mean is

$$\frac{\delta\psi}{\psi} = \frac{\delta N}{N} = \frac{\delta F}{F}$$

$$= \left[\frac{9}{2}\cos(\phi - \theta_w) - \frac{1}{f(\theta)}\frac{\partial f}{\partial\theta}\sin(\phi - \theta_w)\right]G(C,c,\phi)(AK). \qquad (73)$$

According to Bragg scattering theory, the amplitude of the modulations in return signal intensity relative to the mean is equal to $\delta\psi/\psi$ and so, from this expression, is proportional to the swell slope AK.

The result given above shows how the swell-induced modulations depend on the viewing direction ϕ relative to the swell and on the distribution of short, locally generated waves about the wind direction θ_w. The angle ϕ between the direction of propagation of the swell and the direction of viewing can be determined directly from the SAR imagery, but the direction of the local wind cannot. This requires either a simultaneous scatterometer measurement at shorter wavelengths or some independent information about the local meteorology. The phase speed C of the swell can be deduced from the wavelength of the observed swell pattern and the mean phase speed c of the scatterers by a knowledge of the Bragg wavelength. Equation (73) does not explicitly involve the local wind speed, though clearly there are limits to the range of wind speeds over which it is applicable. The wind must be sufficiently strong to generate locally short waves at the Bragg scattering wavelength but not so large that the dominant locally generated waves have orbital velocities comparable with those of the swell. In this latter case, the modulation of the short waves by the longer, locally generated waves may be dominant but, being on a scale smaller than the resolution distance of the SAR, will not be observed. Beal (Ref 34) gives a range of 2 m/s $< U_{10} <$ 10 m/s (where U_{10} is the wind speed at 10 m above the mean sea surface) over which swell-induced modulations have been detected.

An ideal observing situation would be one in which $\theta_w \simeq \phi \simeq 0°$ with swell moving in the viewing direction and a following (or opposing) local wind. The relative modulation amplitude then reduces simply to

$$\frac{\delta\psi}{\psi} = 4.5AK \ . \qquad (74)$$

---

34. R.C. Beal, "Spaceborne imaging radar: monitoring of ocean waves," Science, 208, 1980, 1373-1375.

As ϕ increases from zero, since C >> c in the last factor of Eq (73), the modulation amplitude decreases, reaching a minimum near $\pi/2$. This is consistent with Beal's remark (Ref 34) that the swell can be imaged successfully when there is a substantial component of the swell traveling along the line of sight of the radar.

The first factor in Eq (73) involves the spectral distribution of the short locally generated wind waves that provide the surface scatterers, the first term representing the consequences of variations in wavenumber magnitude and the second in local short wave direction. The directional distribution of the short gravity components in a wind-generated wave field is discussed in Section II.E. Unless the directional distribution of these waves is very narrow, however, the second term is likely to be numerically rather smaller than the first, especially when $(\phi - \theta_w)$ is small. Under these circumstances, a simplified form of Eq (73) may be useful in estimating the swell slope AK directly from satellite measurements.

In an experimental paper Evans and Shemdin (Ref 35) observe that the modulation of short waves by swell is found to be strong enough to be an important component of SAR image formation for the swell. Phillips (Ref 1, p 97-98) presents some further analysis of the action of swell moving across the sea surface. He observes that if the augmented drift U of Eq (59) near the swell crests approaches the local phase speed c of the short waves, the latter may be suppressed entirely. This effect was apparently observed first

---

35. D.D. Evans and D.H. Shemdin, "An investigation of the modulation of capillary and short gravity waves in the open ocean," J. Geophys. Res., 85, 1980, 5019-5024.

by Mitsuyasu (Ref 36) and analyzed by Phillips and Banner (Ref 37), who also conducted further laboratory measurements.

The dispersion relation for short waves is $\sigma = (g'k)^{\frac{1}{2}}$ [see Eq (4) and (60)], and for short waves in the frame of reference of the swell, Eq (1) and (2) give

$$\sigma + k(U - C) = \text{const.} \tag{75}$$

If c_o is the short wave speed at the point $\chi = \pi/2$, where the surface displacement of the swell is zero (remember that $\chi = 0$ at the swell crest) and k_o is the corresponding wavenumber,

$$\begin{aligned}(g'k)^{\frac{1}{2}} + k(U - C) &= (gk_o)^{\frac{1}{2}} - k_o C \\ &= k_o(c_o - C) \\ &= g(c_o - C)/c_o^2 \ .\end{aligned} \tag{76}$$

This is a quadratic in $k^{-\frac{1}{2}}$, or equivalently in $c = (g'/k)^{\frac{1}{2}}$, and since $U = U_o$ and $\cos \chi = CAK \cos \chi$, it can be written as

$$\frac{1 - \alpha}{\alpha^2(1 - AK \cos \chi)}\left(\frac{c}{C}\right)^2 + \left(\frac{c}{C}\right) - (1 - AK \cos \chi) = 0 \ , \tag{77}$$

where $\alpha = c_o/C \ll 1$. Since $c/C \to \alpha$ when $\chi \to \pi/2$, the appropriate root is

$$c/C = \alpha(1 - AK \cos \chi) \ . \tag{78}$$

---

36. H. Mitsuyasu, "Interactions between water waves and wind (I)," Rep. Res. Appl. Mech., Kyushu University, 14, 1966, 67-88.

37. O.M. Phillips and M.L. Banner, "Wave breaking in the presence of wind drift and swell," J. Fluid Mech., 66, 1974, 625-640.

Note that the phase speed c of the short waves is reduced as the crest is approached, while the ambient drift q increases. Consequently the ratio q/c increases and the maximum height of an unbroken wavelet decreases. The maximum amplitude that wavelets can have when they are at the point of incipient breaking at the swell crest is, from Eq (3.9.6) of Ref 1,

$$\zeta_{max} = (2g')^{-1}(c_c - q_c)^2 \ , \tag{79}$$

where $c_c = c_o(1 - AK)$ is the phase speed of the short wave at the swell crest, and q_c is the augmented value of the drift at this point, given in Eq (3.9.4) of Ref 1 as

$$q_c = (C - U_o) - [(C - U_o)^2 - q_o(2C - q_o)]^{\frac{1}{2}} \ . \tag{80}$$

The ratio r of the maximum wavelet amplitude to its maximum in the absence of the swell is, from Eq (3.9.6) of Ref 1 and Eq (79),

$$r = \frac{g}{g'} \frac{(c_c - q_c)^2}{(c_o - q_o)^2} \ , \tag{81}$$

which is an algebraic function of the three parameters $\alpha = c_o/C$, $AK = U_o/C$ and $\gamma = q_o/C$. Measurements by Mitsuyasu (Ref 36) and Phillips and Banner (Ref 37) on the suppression of short wind-generated waves in the laboratory by longer, mechanically generated swell gave good agreement with Eq (81) over the rather limited range of conditions studied.

E. INTERACTION OF SURFACE AND INTERNAL WAVES

1. Introduction

Qualitative relations for the behavior of short surface waves interacting with internal waves are found in Ref 1, p 78-81, 230-232, Ref 23, and Ref 38. Lewis, Lake, and Ko (Ref 24) do a one-dimensional theoretical analysis of a tank experiment. They demonstrate that the normalized amplitude and slope modulations increase with the interaction distance and that the maximum interaction effect occurs when the phase speed of the internal wave equals the group speed of the surface wave. Hughes (Ref 17) produced a theoretical model that showed promising agreement with the experimental results of Ref 39. Holliday (Ref 32) shows that the "wave barrier" noted by Gargett and Hughes (Ref 38) for infinitesimal gravity waves on a slowly varying current from an internal wave is removed by considering finite amplitude effects.

This section considers in detail the results of Phillips (Ref 1, p 78-81, and Ref 23), Lewis, Lake, and Ko (Ref 24); and Hughes (Ref 17). First, the Phillips approach is given. It considers the blockage of surface waves by interaction with internal waves. In the absence of blockage, when energy packets move continuously across the surface, he finds that a steady state can be obtained in which the energy ratio for surface is given by Eq (88). He then proceeds to show that when the wide spectral range of wind-generated waves is considered, the blockage singularity at $U + \frac{1}{2}c - C = 0$ in Eq (88) vanishes and Eq (93) results. Finally, he considers the problem from the

---

38. A.E. Gargett and B.A. Hughes, "On the interaction of surface and internal waves," J. Fluid Mech., 52(1), 1972, 179-191.

39. B.A. Hughes and H.L. Grant, "The effect of internal waves on surface wind waves. 1: Experimental measurements," J. Geophys. Res., 83, 1978, 443-454.

point of view of weak wave-wave interactions and finds the resonance condition of Eq (96).

Next the Ko approach is reviewed. To model the Lewis, Lake and Ko (Ref 24) tank experiment he begins with the appropriate one-dimensional forms of Eq (1) and (7), applies the characteristic Eq (102) and, through a perturbation analysis, obtains Eq (129) and (130). Both the theoretical and experimental results for slope and amplitude modulations show that, when normalized by the ratio of induced surface current to internal wave phase speed (ie, u_o/C), the resonant case (ie, internal wave phase speed C matches the surface wave group speed c_{go}) modulation magnitudes are dependent only on the interaction distance and are independent of the magnitudes of the other physical parameters. Likewise, the maximum normalized slope and amplitude interaction effects are found to occur when $C = c_{go}$.

Finally Hughes' approach is treated. The Hughes (Ref 17) model is designed for comparison with the experimental results of Ref 39. He begins with the appropriate forms of Eq (1), (2), and (4) with a source term added to the latter. This is Eq (133), which he manipulates to a form of Eq (8) in Eq (134), with the source term given by Eq (135), which is a form of the first three terms $\sum_{i=1}^{3} S_i$ of Eq (22)-(24). After some manipulation he arrives at Eq (140), which is a simplified form of the radiative transfer equation in terms of the action spectrum. From this, to the first order in $|U|/C$, he obtains Eq (143c). Expressing the internal wave surface speed U as a sum of different internal wave wavenumber components [Eq (144)], he then obtains Eq (145) for the wave displacement spectrum $\psi(k_1,k_2)$, from which he obtains some quantities which he can compare with the experimental results of Ref 39. The resulting comparison of theory and experimental results is encouraging.

2. Phillips' Approach

The Phillips approach to the modulations in surface waves induced by internal waves is given in Ref 1 and 23 (p 78-81). When long internal waves of the kind described in Section 5.3 of Ref 1 propagate with velocity $\underline{C}$ along the oceanic thermocline, the orbital motion near the surface is oscillatory, in essence horizontal and of the form $\underline{U}[\underline{K}\cdot(\underline{x} - \underline{C}t)]$, where $\underline{K}$ is the wavenumber of the internal wave. As far as short surface waves are concerned, provided that their wavenumber $k >> K$, the disturbance current induced by the internal wave is independent of depth within the range $|kz| \lesssim 1$ and has a horizontal length scale (the internal wave wavelength) that is very much greater than their own wavelength. The methods of Section 3.6 of Ref 1 can then be applied to such a train of short surface waves as they are modified by the moving current distribution $\underline{U}[\underline{K}\cdot(\underline{x} - \underline{C}t)]$, supposed known.

The algebra is simplest when the two wave trains are collinear. In a frame of reference moving with the internal wave, the pattern of surface waves when steady gives, from Eq (1) and (2),

$$\sigma - k(C - U) = \text{const.} = \sigma_o - k_o C \ , \tag{82}$$

where $\sigma_o = (gk_o)^{\frac{1}{2}}$ is the surface wave intrinsic frequency at the phase point of the internal wave, where the induced current vanishes. This equation can be written as a quadratic in c/c_o with the solution

$$\frac{c}{c_o} = [2(c_o - C)]^{-1} \left\{ c_o + (c_o - C) \left[1 + \frac{4U(c_o - C)}{(c_o - 2C)^2} \right]^{\frac{1}{2}} \right\} \tag{83}$$

which is real, provided

$$U \geq -\frac{(c_o - 2C)^2}{4(c_o - C)} \ . \tag{84}$$

If at some point equality occurs,

$$\frac{c}{c_o} = \frac{c_o}{2(c_o - C)} \tag{85}$$

and it can be shown that $\frac{1}{2}c + U - C = 0$. Relative to the internal wave pattern, the energy flux of the surface wave vanishes. Note that if the undisturbed group speed approaches the phase speed C of the internal waves, it appears from Eq (84) that an arbitrary small adverse current is sufficient to induce blockage.

The distribution of wave energy can be found from the action conservation principle. In a frame of reference moving with the speed C of the current pattern, Eq (5) becomes

$$\frac{\partial}{\partial t}\left(\frac{E}{\sigma}\right) - \frac{\partial}{\partial x}\left[(U + c_g - C)\frac{E}{\sigma}\right] = 0 \ . \tag{86}$$

For a steady wave train, since $\sigma = g/c$,

$$Ec(U + \tfrac{1}{2}c - C) = \text{const.} = E_o c_o(\tfrac{1}{2}c_o - C) \ , \tag{87}$$

where E_o is the energy density at the phase point of the internal wave, where $U = 0$. As U varies with respect to the phase of the internal wave, the local phase speed c varies also as specified by Eq (83), with corresponding modulations in the energy density. Near a blockage point, $U + \frac{1}{2}c - C \to 0$ and from Eq (87), the steady-state solution requires an indefinitely large wave energy density and evidently fails. From a given initial state, a time-dependent solution can, of course, be calculated numerically from Eq (1) and (86). In the absence of blockage, when energy packets move continuously across the surface, a steady state can be obtained in which the energy ratio of the surface waves is

$$\frac{E}{E_o} = \frac{c_o(\tfrac{1}{2}c_o - C)}{c(U + \tfrac{1}{2}c - C)} \tag{88}$$

in agreement with an expression given by Gargett and Hughes (Ref 38) for this case. The singularities in the energy density that occur in Eq (88) if the denominator vanishes are clearly associated with the kinematic limits, described previously, when the energy propagation speed relative to the moving pattern vanishes or when the phase speed itself vanishes and the wavenumber tends to infinity. Under either of these conditions, the steady-state solution will fail. The time-dependent Eq (86) becomes, at the points on the surface where $U + c_g - C = 0$,

$$\frac{\partial E}{\partial t} = -\frac{\partial U}{\partial x}E \ . \tag{89}$$

Accordingly, $E = E_o e^{-at}$, where E_o is the energy density at the blockage point at time $t = 0$ and a represents the rate of surface divergence at this point. If a is negative (at a convergence point) the energy density increases monotonically.

The analysis to this point has been concerned with a single train of waves, slowly varying in space and time as a result of the interactions with the current distribution. Wind-generated waves, however, extend over a wide spectral range, and the previous results can be extended to describe this situation. When the surface waves are sufficiently two-dimensional, simple analytical results can be derived directly from the solutions given above. If F(k) represents the spectral density in the wave field, then the energy contained in the wavenumber band dk is F(k)dk. The total energy content (per unit area) is specified in the steady state in terms of the energy content F(k)dk of the band in its undisturbed state by Eq (88):

$$\frac{F(k)dk}{F_o(k)dk_o} = \frac{c_o(\tfrac{1}{2}c_o - C)}{c(U + \tfrac{1}{2}c - C)} \tag{90}$$

Note that the width of the band varies with x as well as the energy density. The variation can be found from Eq (82) in the form

$$k[(g/k)^{\frac{1}{2}} + U - C] = k_o[(g/k_o)^{\frac{1}{2}} - C] \ . \tag{91}$$

Taking differential increments in the wavenumber k and k_o for a given U and C gives

$$\frac{dk}{dk_o} = \frac{\tfrac{1}{2}c_o - C}{\tfrac{1}{2}c + U - C} \ . \tag{92}$$

The combination of Eq (90) and (92) leads to the surprising simple result

$$\frac{F(k)}{F(k_o)} = \frac{c_o}{c} = \left(\frac{k}{k_o}\right)^{\frac{1}{2}} \ . \tag{93}$$

An interesting property of this expression is that the singularity in Eq (90), when the net group speed vanishes, has disappeared from Eq (93). The reason for this is that the range of wavenumbers about the critical value at the kinematic limit becomes large, as does the energy content, so that the energy density in wavenumber space remains finite. The singularity when $c \to 0$ remains, though for situations of interest in this section, this limitation is not encountered.

It is instructive to examine briefly the same example from the point of view of the resonant interactions discussed in Section 2.8 of Ref 1. Two surface wave trains with wavenumbers k_1, k_2 can form a resonant triad with a collinear internal wave with wavenumber $k_3 = K$, provided the conditions

$$k_1 = k_2 + k_3 \ , \quad \sigma_1 = \sigma_2 + \sigma_3 \ , \tag{94}$$

where σ_3 is the frequency of the internal wave, are satisfied. Since the wavelength of the internal wave is very much greater than those of the surface waves, $k_3 = K << k_1, k_2$, and the difference $k_1 - k_2 = \delta k$ between the two surface wavenumbers is very small. If $\sigma_1 - \sigma_2 = \delta\sigma$, the resonance conditions of Eq (94) are

$$\delta k = k_3 \ , \quad \delta\sigma = \sigma_3 \tag{95}$$

so that

$$\frac{\delta\sigma}{\delta k} = \frac{\sigma_3}{k_3} \text{ or } c_g = C \ . \tag{96}$$

For resonance, the phase speed of the internal wave is equal to the group speed of the surface wave. This is identical to the condition for blockage with an internal wave of small amplitude. Under these conditions a steady-state solution is not possible. Energy resident initially in a uniform surface wave train with wavenumber k_1 flows to a neighboring wavenumber $k_1 - \delta k$ (and to the internal wave). The wave train develops modulations on the scale of the internal wave, their amplitude continually increasing with time.

The resonant generation of internal waves by nonlinear interactions with surface waves has been studied by Brekhovskikh, et al (Ref 40). This theory predicts that an initially uniform surface wave, in the presence of an internal wave such that Eq (96) is satisfied, will develop growing modulations as an additional Fourier component of the surface wave with an adjacent wavenumber (the third member of the triad) is generated. The two types of approach are clearly complementary at this point. However, the assumption of a slowly varying wave train is unable to cope with a situation in which two quite different Fourier components of the surface wave are involved. In the

---

40. L.M. Brekhovskikh, et al, "On the resonant generation of internal waves through nonlinear interactions of surface waves," Bull. (Dzv.) Acad. Sci. USSR, Atmos. and Oceanic Phys., 8, 1972, 192.

same way, the simple resonance theory is not well suited to consider the blockage phenomenon that occurs when $C - c_g$ is not small and the adverse current is substantial.

3. Ko's Approach

The Ko approach to the interaction of internal waves and surface gravity waves is given in Ref 24. He defines the internal wave induced fractional changes in surface wave amplitude a and slope m as follows:

$$a_* \equiv \frac{a_{max} - a_{min}}{a_{max} + a_{min}} \tag{97}$$

and

$$m^* = \frac{m_{max} - m_{min}}{m_{max} + m_{min}} . \tag{98}$$

Instead of a general solution to Eq (1) and (9) for this problem, this study was directed toward the one-dimensional wave interaction corresponding to their tank experiment. The surface current U from the internal wave is generated by the interfacial waves of a two-fluid system with frequency Ω and phase speed C for time $t > 0$. An independent surface wave generator with frequency ω is used to produce for all time a single surface wave train with wavenumber k_o and unperturbed group speed c_{go}. The problem was to determine the change in the surface wave characteristics as functions of both position x along the tank and time t, when the internal wave induced surface current field U was present.

For these one-dimensional waves, the governing relations, ie, Eq (1) and (7), were simplified as follows. Equation (1) became

$$\frac{\partial k}{\partial t} + (c_g + U)\frac{\partial k}{\partial x} = -k\frac{\partial U}{\partial x} , \tag{99}$$

where $c_g = \frac{1}{2}(g/k)^{\frac{1}{2}}$ and $U = U(x,t)$. Equation (7) reduced to

$$\frac{\partial A^2}{\partial t} + \frac{\partial}{\partial x}\left[(c_g + U)A^2\right] = -\tfrac{1}{2}A^2\frac{\partial U}{\partial x} , \tag{100}$$

which was written in the alternative form

$$\frac{\partial A^2}{\partial t} + (c_g + U)\frac{\partial A^2}{\partial x} = -\frac{3}{2}A^2\frac{\partial U}{\partial x} - A^2\frac{\partial c_g}{\partial x} . \tag{101}$$

Both Eq (99) and (101) were written in a characteristic form for which the solution could be readily obtained. These characteristics were defined by

$$\frac{dx}{dt} = c_g + U , \tag{102}$$

for which the two governing equations reduce to

$$\frac{dk}{dt} = -k\frac{\partial U}{\partial x} \tag{103}$$

and

$$\frac{dA^2}{dt} = -\frac{3}{2}A^2\frac{\partial U}{\partial x} - A^2\frac{\partial c_g}{\partial x} . \tag{104}$$

In other words, in the characteristic coordinate system defined by integrating Eq (102) such that $x = x(\tau,\xi)$, $t = \tau$, where ξ = constant denotes a characteristic, the governing equations [Eq (103) and (104)] become

$$\left.\frac{\partial \ell n k}{\partial \tau}\right|_{\xi} = \left.-\frac{\partial U}{\partial x}\right|_{t} \tag{105}$$

and

$$\left.\frac{\partial \ell n A^2}{\partial \tau}\right|_{\xi} = \left.-\frac{3}{2}\frac{\partial U}{\partial x}\right|_{t} - \left.\frac{\partial c_g}{\partial x}\right|_{t} \tag{106}$$

To simulate the tank experiment the surface current field was represented by

$$U = u_o \sin K(x - Ct)H(x)H(t - x/C) \ , \tag{107}$$

where H(x) represents the Heaviside function.

To simplify the analysis further, it was assumed that the magnitude of the surface current u_o was small compared with the minimum of the group speed for surface waves, ie,

$$\varepsilon \equiv u_o/c_{go} << 1 \ , \tag{108}$$

where $c_{go} = \frac{1}{2}(g/k_o)^{\frac{1}{2}}$, the unperturbed group speed. Then it was assumed that the solutions could be represented by the following perturbation series in ε:

$$\begin{aligned} x &= x_o + \varepsilon x_1 + \varepsilon^2 x_2 + \ldots \ , \\ \ell nk &= \ell nk_o + \varepsilon \ell nk_1 + \varepsilon^2 \ell nk_2 + \ldots \ , \\ \ell nA^2 &= \ell nA_o^2 + \varepsilon \ell nA_1^2 + \varepsilon^2 \ell nA_2^2 + \ldots \ , \\ c_g &= c_{go} + \varepsilon c_{g_1} + \varepsilon^2 c_{g_2} + \ldots \ , \end{aligned} \tag{109}$$

where $c_{g_1} = -\frac{1}{2}c_{go} \cdot \ell nk_1$.

Substituting Eq (109) into Eq (102), (105), and (106) and grouping terms of the same order in ε gave for $0(\varepsilon^0)$:

$$\frac{\partial x_o}{\partial \tau} = c_{go} \ , \quad \frac{\partial k_o}{\partial \tau} = 0 \ , \quad \frac{\partial A_o^2}{\partial \tau} = -A_o^2 \frac{\partial c_{go}}{\partial x} = 0 \ . \tag{110}$$

These equations describe the unperturbed surface wave field, which was assumed to be a uniformly generated monochromatic wave train. Integration of Eq (110) gives

$$k_o = \text{const.}, \ A_o^2 = \text{const.}, \ x_o = c_{go}(\tau - \xi) \ , \tag{111}$$

where ξ denotes the intersection of the characteristic with the t axis. For $O(\varepsilon)$ the governing equations become

$$\varepsilon\frac{\partial \ell n k_1}{\partial \tau} = u_o[K \cos K(x_o - Ct)H(x_o)H(t - x_o/C) + \sin K(x_o - Ct)\delta(x_o)H(t - x_o/C) - C^{-1} \sin K(x_o - Ct)H(x_o)\delta(t - x_o/C)] , \quad (112)$$

$$\frac{\partial \ell n A_1^2}{\partial \tau} = \frac{3}{2}\frac{\partial \ell n k_1}{\partial \tau} - \frac{\partial c_{g_1}}{\partial x} , \quad (113)$$

and

$$\varepsilon\frac{\partial x_1}{\partial \tau} = u_o \sin K(x_o - Ct)H(x_o)H(t - x_o/C) + \varepsilon c_{g_1} , \quad (114)$$

where $\varepsilon \ell n k_1$ and $\varepsilon \ell n A_1^2$ represent the first-order change of the wavenumber and the square of the amplitude, respectively, while εx_1 gives the deviation from the unperturbed characteristic.

Using the zeroth-order characteristic gives

$$x_o - Ct = (c_{go} - c)\tau - c_{go}\xi . \quad (115)$$

Then the equations could be integrated from $\tau = 0$ to τ along a given characteristic ξ = const. The solution to Eq (112) was obtained first, then used on the right-hand sides of Eq (113) and (114). The solution for the wavenumber is given by

$$\varepsilon \ell n k_1 = \ell n\frac{k}{k_o} = -\frac{u_o}{c_{go} - C}H(x_o)\left[\sin K(x_o - Ct)H(t - x_o/C) - \frac{C}{c_{go}} \sin KC\left(\frac{x_o}{c_{go}} - t\right)H(t - x_o/c_{go})\right] , \quad (116)$$

and for the amplitude by

$$\ell n\frac{A}{A_o} = -\frac{1}{4}\frac{u_o}{c_{go} - C}H(x_o)\left\{\left(3 + \frac{c_{go}}{c_{go} - C}\right)\sin K(x_o - Ct)H(t - x_o/C)\right.$$

$$-\frac{C}{c_{go}}\left[\left(4 + \frac{c_{go}}{c_{go} - C}\right)\sin KC\left(\frac{x_o}{c_{go}} - t\right)\right.$$

$$\left.\left. + \frac{C}{c_{go}}Kx_o \cos KC \cos KC\left(\frac{x_o}{c_{go}} - t\right)\right] H\left(t - \frac{x_o}{c_{go}}\right)\right\}. \quad (117)$$

For $k = k_o + \Delta k$ and $A = A_o + \Delta A$, the right-hand sides of Eq (116) and (117) give the changes in wavenumber ($\Delta k/k_o$) and wave amplitude ($\Delta A/A_o$), respectively, for small changes. In practice, their interest was in the change of the local surface wave slope, which is related to the changes in wavenumber and amplitude by

$$\ell n\frac{m}{m_o} = \ell n\frac{k}{k_o} + \ell n\frac{A}{A_o}\ , \quad (118)$$

or for small variations by

$$\frac{\Delta m}{m_o} = \frac{\Delta A}{A_o} + \frac{\Delta k}{k_o}\ . \quad (119)$$

They found it interesting to also calculate the maximum changes in the surface wavenumber, the amplitude and the slope at a given x-station, as well as the corresponding phase of the interval wave current where the maximum effect occurs. For the region where both Heaviside functions in Eq (116) and (117) are equal to 1, it is appropriate to drop the Heaviside function notation. Furthermore, they define

$$\phi = K(x_o - Ct) \quad (120)$$

and

$$\theta = KC\left(\frac{x_o}{c_{go}} - t\right) = \phi - B \tag{121}$$

with

$$B = Kx_o(1 - C/c_{go}) \ . \tag{122}$$

Then Eq (116), (117) and (118) can be rewritten as

$$\ell n\frac{k}{k_o} = - \frac{u_o}{c_{go} - C}\left[\sin \phi - \frac{C}{c_{go}} \sin \theta\right] \ , \tag{123}$$

$$\ell n\frac{A}{A_o} = - \frac{1}{4} \frac{u_o}{c_{go} - C}\left[\left(3 + \frac{c_{go}}{c_{go} - C}\right) \sin \phi \right.$$

$$\left. - \frac{C}{c_{go}} \left\{\left(4 + \frac{c_{go}}{c_{go} - C}\right) \sin \theta + \frac{C}{c_{go}} Kx_o \cos \theta\right\}\right] \tag{124}$$

and

$$\ell n\frac{m}{m_o} = - \frac{1}{4} \frac{u_o}{c_{go} - C}\left[\left(7 + \frac{c_{go}}{c_{go} - C}\right) \sin \phi \right.$$

$$\left. - \frac{C}{c_{go}} \left\{\left(8 + \frac{c_{go}}{c_{go} - C}\right) \sin \theta + \frac{C}{c_{go}} Kx_o \cos \theta\right\}\right] \tag{125}$$

For a given x_o and C/c_{go}, the maximum or minimum change occurs at ϕ^*, the phase of the internal wave where $\partial()/\partial\phi = 0$; the quantity inside the parentheses can be any one of the three quantities given on the left of Eq (123), (124), and (125). The results of performing the indicated differentiations are

$$\phi_k^* = \tan^{-1}\left(\frac{c_{go}/C - \cos B}{\sin B}\right) , \tag{126}$$

$$\phi_A^* = \tan^{-1}\left\{\frac{3 + \frac{c_{go}}{c_{go} - C} - \frac{C}{c_{go}}\left[\left(4 + \frac{c_{go}}{c_{go} - C}\right)\cos B + \frac{C}{c_{go}}Kx_o \sin B\right]}{\frac{C}{c_{go}}\left[\left(4 + \frac{c_{go}}{c_{go} - C}\right)\sin B - \frac{C}{c_{go}}Kx_o \cos B\right]}\right\} \quad (127)$$

and

$$\phi_m^* = \tan^{-1}\left\{\frac{7 + \frac{c_{go}}{c_{go} - C} - \frac{C}{c_{go}}\left[\left(8 + \frac{c_{go}}{c_{go} - C}\right)\cos B + \frac{C}{c_{go}}Kx_o \sin B\right]}{\frac{C}{c_{go}}\left[\left(8 + \frac{C}{c_{go} - C}\right)\sin B - \frac{C}{c_{go}}Kx_o \cos B\right]}\right\} \quad (128)$$

The corresponding maximum or minimum values are obtained by substituting Eq (126), (127), and (128) into Eq (123), (124), and (125), respectively.

Since the solutions of Eq (116) and (117) appear to be inversely proportional to $C - c_{go}$, a singular behavior may seem probable at resonance. However, with a proper limiting procedure, it can be shown that, for $c_{go} \to C$,

$$\ell n\frac{k}{k_o} = -\frac{u_o}{C}H(x_o)H(t - x_o/C)[\sin K(x_o - Ct) + Kx_o \cos K(x_o - Ct)] \quad (129)$$

and

$$\ell n\frac{A}{A_o} = -\frac{u_o}{4C}H(x_o)H(t - x_o/C)[(4 - K^2x_o^2)\sin K(x_o - Ct) + 5Kx_o \cos K(x_o - Ct)] \quad . \quad (130)$$

Notice the strong dependence of the solution on kx_o, which effectively measures the distance or "time" of interaction. Further, in this model, the energy transfers only from the internal wave, and there is no provision to account for the limited energy available in the internal wave. Without considering the other nonlinear effects and the energy loss of the internal

wave train, the linearized solutions for the resonance case predict a monotonic increase of the effects with distance as shown by Eq (129) and (130).

Both the theoretical and experimental results for slope and amplitude modulations show that, when normalized by the ratio of induced surface current to internal wave phase speed (ie, u_o/C), the "resonant" case (ie, $C \simeq c_{go}$) modulation magnitudes are dependent only on the interaction "distance" kx and are independent of the magnitudes of the other physical parameters. The maximum normalized (by u_o/C) slope and amplitude interaction effects are found to occur, for both theory and experiment, when the phase speed of the internal wave and the group speed of the surface wave are matched (ie, $C = c_{go}$).

4. HUGHES' APPROACH

Hughes (Ref 17) begins with Eq (1), (2), and (5), which in his notation reduce to

$$\frac{\partial k_1}{\partial t} + \frac{\partial}{\partial x}(k_1 U + \sigma) = 0 \tag{131}$$

$$k_2 = \text{const.} \tag{132}$$

$$\frac{\partial A}{\partial t} + \frac{\partial}{\partial x}[A(U + c_g)] = \Lambda_1 \ , \ c_g = \frac{\partial \omega}{\partial k_1} \tag{133}$$

Note that he has added a source (or "growth/decay") term, which, we shall see, leads to $\sum_{i=1}^{n} S_i$ of Eq (19). By manipulation of his variable dependence, he arrives at Eq (8) in the form

$$\frac{\partial N}{\partial x} + (U + c_g)\frac{\partial N}{\partial x} = \Lambda \tag{134}$$

where he uses

$$\Lambda = \sum_{i=1}^{3} S_i = \alpha(k_1,k_2) + \beta(k_1,k_2)N - \gamma(k_1,k_2)N^2 \qquad (135)$$

in place of the relations in Section II.E. He justifies ignoring $\alpha(k_1,k_2)$ and observes that the third term represents a nonlinear limitation to the exponential growth, and while it does not allow for overshoot effects, it does provide an inherent upper limit to the spectral growth.

Let k_o be the initial value of k_1 in the sense that $k_1(k_o,x,t) = k_o$ at $x = t = 0$. If the wave spectrum in the absence of interaction is stationary or growing/decaying very slowly, the left side of Eq (134) is zero; therefore at equilibrium, $\Lambda = 0$, so that

$$\gamma(k_o,k_2) = \beta(k_o,k_2)/N_o \ , \qquad (136)$$

where $N_o(k_o,k_2)$ is the unperturbed equilibrium spectral value. It is also assumed that this condition holds for perturbed wave numbers, ie, during surface–internal wave interaction, but with k_o replaced by k_1. This is equivalent to assuming that the wind shifts the spectral amplitude for given $\underline{k}$ toward the equilibrium spectral amplitude of the same wavenumber. Under these conditions, Eq (134) becomes

$$\frac{\partial N}{\partial t} + [U(x,t) + c_g]\frac{\partial N}{\partial x} = \beta(k_1,k_2)N - \frac{\beta N^2}{N_o(k_1,k_2)} \ . \qquad (137)$$

To complete the mathematical statement of the problem, ie, Eq (131), (132), and (136), initial conditions on k_1 and N are imposed:

$$k_1(t = 0,x,y) = k_o$$
$$N(t = 0,x,y) = N_o(k_o,k_2) \ . \qquad (138)$$

Using the method of characteristics on Eq (131), k_1 can be obtained by solving the pair of coupled nonlinear first-order ordinary differential equations

$$\frac{dx}{dt} = U(x,t) + c_g$$

$$\frac{dk_1}{dt} = -k_1 \frac{\partial U}{\partial x}\bigg|_{x=x(t)} , \tag{139}$$

where $x(0)$ is arbitrary. Along the path $x(t)$ with $k_1(t)$ known (in principle), Eq (137) becomes

$$\frac{dN}{dt} = \beta[k_1(t),k_2]N - \beta^2 N^2/N_o[k_1(t),k_2] , \tag{140}$$

which is just a particular form of Eq (9). Equation (140) is a simplified form of Eq (19), whose solution, after integrating once by parts on η and using Eq (139), is

$$N(k_1(t),k_2) = N_o[k_1(t),k_2] \left\{ 1 - N_o\,[k_1(t),k_2] \int_o^t \frac{k_1}{\psi_o(k_1(\eta),k_2} \right.$$

$$\left. \cdot \frac{\partial \psi_o}{\partial k_1} \left(\frac{\partial U}{\partial x}\right)_{x(n)} \exp\left(- \int_\eta^t \beta(k_1(q),k_2)dq \right) d\eta \right\}^{-1} . \tag{141}$$

If the orbital velocity of the internal waves is represented by $U = U(x - Ct)$, where C is the phase velocity of the internal wave, then trapped waves exist between locations where

$$c_g + U(x - Ct) - C = 0 \tag{142}$$

as described in Ref 38 and in Ref 1, p 78-81. Hughes (Ref 17) discussed some properties of the solution of Eq (141), including the trapped waves.

Hughes (Ref 17) next considers only steady, dispersionless current fields. Therefore, he particularizes the theory to the case of $U = U(x - Ct)$ and $|U|/C \to 0$. If all powers of $|U|/C$ except the first are ignored, Eq (139) and (141) have the solution

$$x = x_o + c_{go}t + O(U) \tag{143a}$$

$$k_1 = k_o \left(1 - \int_o^t U'[x_o + (c_{go} - C)\eta]d\eta\right) \tag{143b}$$

$$N(k_1,k_2) = N_o(k_1,k_2) + k_1\frac{\partial N_o}{\partial k_1} \int_o^t U'[x_o - (c_g - C)\eta] \cdot \exp\,[-\beta(k_1,k_2)(t - \eta)]d\eta, \tag{143c}$$

where $U' = \dfrac{\partial U}{\partial x}$ and $c_{go} = \left(\dfrac{\partial \omega}{\partial k_1}\right)_{k_o}$.

In terms of the wave displacement spectrum ψ, with U expressed as a sum of different internal wave wavenumber components, ie,

$$U(x,t) = \sum_{n=1}^{N} B_n \sin\,[K_n(x - Ct) + \theta_n]\ , \tag{144}$$

the integration can be carried out to yield

$$\psi(k_1,k_2) = \psi_o(k_1,k_2) + \sum_{n=1}^{N} \frac{B_n \sigma k_1}{C}\frac{\partial N_o}{\partial k_1} \cdot \frac{(\beta/CK_n)C_n(x,t) + (c_g/C - 1)D_n(x,t)}{(\beta/cK_n)^2 + (c_g/C - 1)^2}\ , \tag{145}$$

where for $t \gtrsim 30$ min

$$C_n(x,t) = \cos [K_n(x - Ct) + \theta_n]$$

and

$$D_n(x,t) = \sin [K_n(x - Ct) + \theta_n]. \tag{146}$$

In Eq (145) note that exact resonance occurs when $c_g = C$ and each component of the surface wave field is additively perturbed by each component of the internal wave field (in this approximation).

From ordinary resonance analysis, the phase angle μ_n for each perturbation component is given by

$$\tan \mu_n = \frac{\beta/CK_n}{c_g/C - 1} . \tag{147}$$

and thus for weak damping, μ_n increases from -180° to 0° as c_g increases from much less than C to much greater than C. As $\beta/Ck_n \to 0$, the range of c_g over which μ_n changes appreciably becomes more closely confined to the resonance point $c_g = C$. The phenomenon of trapping is degenerate in this linear approximation, and only those waves that satisfy the resonance condition [Eq (142) with $U/C \to 0$] can be said to be "trapped."

With this description and with a least-squares regression, the sensitivity and phase of the mean square slope can be defined. Let $\overline{s^2}$ represent the total surface slope variance (the sum of the variances of the two slope components). Then

$$\overline{s^2} = \int_{-\infty}^{\infty}\int (k_1^2 + k_2^2)\psi(k_1,k_2)dk_1dk_2 \tag{148}$$

and from Eq (145)

$$C\left(\frac{\overline{s^2} - \overline{s_o^2}}{\overline{s_\delta^2}}\right) = \sum_{n=1}^{N} B_n R_n \sin\left[k_n(x - Ct) + \theta_n + \mu_n\right] \tag{149}$$

$$= \sum_{n=1}^{N} B_n R_n \left\{\sin[k_n(x - Ct) + \theta_n] \cos \mu_n \right.$$

$$\left. + \cos\left[k_n(x - Ct) + \theta_n\right] \sin \mu_n \right\},$$

where R_n and μ_n are, respectively, the sensitivity and phase of the component $\overline{s^2}$ with wavenumber k_n, ie,

$$R_n \cos \mu_n = \frac{1}{\overline{s_\delta^2}} \iint_{-\infty}^{\infty} \sigma k_1 (k_1^2 + k_2^2) \frac{\partial N_o}{\partial k_1} \cdot \frac{(c_g/C - 1)}{(\beta/Ck_n)^2 + [c_g/C - 1]^2} dk_1 dk_2 \tag{150a}$$

$$R_n \sin \mu_n = \frac{1}{\overline{s_\delta^2}} \iint_{-\infty}^{\infty} \sigma k_1 (k_1^2 + k_2^2) \frac{\partial N_o}{\partial k_1} \cdot \frac{\beta/Ck_n}{(\beta/Ck_n)^2 + [c_g/C - 1]^2} dk_1 dk_2 \; . \tag{150b}$$

In accordance with the measurement process, an overall sensitivity R and phase μ may be determined by correlating the perturbations in $\overline{s^2}$ with phase-shifted current values and defining μ as the phase shift that maximizes the correlation and R as the corresponding regression line slope. By performing the required manipulations to Eq (144) and (139), it can be shown that

$$\tan \mu = \sum_{n=1}^{N} B_n{}^2 R_n \sin \mu_n \left(\sum_{n=1}^{N} B_n{}^2 R_n \cos \mu_n \right)^{-1} \tag{151a}$$

and

$$R = \left[\left(\sum_{n=1}^{N} B_n{}^2 R_n \cos \mu_n\right)^2 + \left(\sum_{n=1}^{N} B_n^2 R_n \sin \mu_n\right)^2\right]\left(\sum_{n=1}^{N} B_n{}^2\right)^{-1} \qquad (151b)$$

Values for R_n and μ_n are obtained by evaluating the integrals given in Eq (150), but before this can proceed it is necessary to estimate $\psi_o(k_1,k_2)$ for each data set.

Measured values of ψ integrated in angle at various values of x,t within the internal wave field can also be obtained. That is, with $k_1 = k \cos \theta$, $k_2 = k \sin \theta$ and $H(k) = \int_o^{2\pi} d\theta \psi(k,\theta)$,

$$H(k) = H_o(k) + \sum_{n=1}^{N} \frac{B_n k\sigma}{C} \int_o^{2\pi} d\theta \cos \theta \frac{2N_o}{(\partial(k \cos \theta)} \cdot \left[\frac{(\beta/Ck_n)C_n(x,t) + (c_g/C - 1)D_n(x,t)}{(\beta/Ck_n)^2 + (c_g/C - 1)^2}\right], \qquad (152)$$

where

$$\beta = \sigma[(u_* \cos \theta/c]\{0.01 + 0.016 \cdot |\cos \theta| \cdot u_*/c\} \cdot \{1 - \exp[-8.9(u_*/c - 0.03)^{\frac{1}{2}}]\} \qquad (153)$$

and θ is the angle between the surface wave propagation and the wind direction.

The theoretical and measured values of the sensitivity gave good agreement, while for the phase μ the agreement was poor except that all theoretical and measured values lay in the same quadrant. An illustration of the agreement between the theoretical and measured forms for the integrated spectrum H(k) is given in Fig 4 of Ref 17. The agreement was satisfactory except at high wavenumbers.

F. WAVE ATTENUATION

Wave attenuation coefficients are found in Ref 1, p 51-54. The simplest case is that of deep water and a clean surface. Although the viscous stresses in the surface layer are important, the layer itself makes a negligible contribution to the overall rate of energy dissipation since the rates of strain there are no larger than in the irrotational flow and the layer thickness is small. The energy losses arise almost entirely from the straining of the irrotational motion, so that the attenuation coefficient is

$$\gamma_v = 2\nu k^2 \ , \tag{154}$$

where the kinematic viscosity of water is $\nu \simeq 0.01$ $cm^{-1}sec^{-1}$ at 20°C and $35°/_{oo}$ salinity. The energy density of the wave field decreases as $\exp(-2\gamma_v t)$ and the amplitude as $\exp(-\gamma_v t)$.

With a densely packed surface film, the attenuation factor γ_f resulting from the surface layer alone is now

$$\gamma_f = \tfrac{1}{2}\nu k\sqrt{\sigma/2\nu} \tag{155}$$

in deep water. The variation of γ_v and γ_f with wavelength and frequency is illustrated in Fig 3.1 of Ref 1. It is evident that, except for the very short capillaries, $\gamma_f >> \gamma_v$. Short waves incident upon a slick are quite rapidly attenuated and, since the apparent smoothness of the sea surface is very much dependent on small-scale components, this attenuation evidently accounts for the smooth appearance of oil slicks in the ocean.

IV. PRELIMINARY CONCLUSIONS AND RECOMMENDATIONS

The purpose of this study of the state of the art of sea surface modeling was to determine the feasibility of designing a software model that could adequately describe the sea surface for treating (1) acoustic torpedo surface reverberation in shallow water and (2) remote radar surface imaging. From the above material we come to the preliminary conclusion that such a sea surface software model is presently possible. We now outline how such a software model might be developed and implemented.

The basic tool for the sea surface model would be the radiative transfer equation, Eq (19), as described in Section II.F. Since, as seen in Section III, the interaction of surface and internal waves is the best-understood phenomenon, this provides a good area in which to start developing our sea surface software model. First, the radiative transfer relation of Ref 17 would be implemented based on the information contained in Section III.E.4. This would be compared with the experimental results of Ref 39 (Section III.E.4) and Ref 24 (Section III.E.3). Then additional radiative transfer source terms from Section II.F would be included and the experimental comparison would be repeated. As a further check, the model would be reconciled with Eq (88) and (93).

Next the model would be extended to agree with the JONSWAP spectrum of Eq (27) and the directional relation of Eq (17). Then the model would be generalized to consider variable surface currents and checked against Eq (41), (43), (49), and (58). Finally swell conditions would be added and tests made against Eq (73). At this point all four phenomena of interest (ie, wind velocity, surface currents, swell, and internal waves) would be present in the development.

To be useful for the stated naval system problem modeling, the sea surface software model should be treated to yield the spectra for slopes, velocities, and accelerations and then extensively tested by varying the many variables and checking the results. The material following Eq (148) presents an interesting area of experimental verification for slope properties, as does the information in Ref 24, Section III.E.3.

The total software package for the statistical modeling of the sea surface would then be ready for application to modeling the acoustic torpedo surface reverberation in shallow water and remote radar sea surface imaging. This would be accomplished by formulating (1) software that gives a statistical description of surface reverberation and (2) software that gives a statistical description of imaging for remote radar sensing. The latter should be extended to address the phenomena of the directional attenuation of surface wave trains and solitary waves.

REFERENCES

1. O.M. Phillips, The Dynamics of the Upper Ocean, Cambridge University Press, 1977.

2. F. Unsell, "Steady wave patterns on a non-uniform fluid flow," J. Fluid Mech., 9, 1960, 333-346.

3. G.B. Whitham, "A note on group velocity," J. Fluid Mech., 9, 1960, 347-352.

4. F.P. Bretherton and C.J.R. Garrett, "Wavetrains in inhomogeneous moving media," Proc. Roy. Soc., A, 302, 1969, 529.

5. F.P. Bretherton, "The general linearized theory of wave propagation," in Mathematical Problems in the Geophysical Sciences, vol. 1, 61-102, Amer. Math. Soc., Providence, RI, 1971.

6. M.S. Longuet-Higgins and R.W. Stewart, "Changes in the form of short gravity waves on long waves in tidal currents," J. Fluid Mech., 8, 1960, 565-583.

7. M.S. Longuet-Higgins and R.W. Stewart, "The changes in amplitude of short gravity waves on steady non-uniform currents," J. Fluid Mech., 10, 1961, 529-549.

8. G.B. Whitham, "Mass momentum and energy flux in water waves," J. Fluid Mech., 12, 1962, 135-147.

9. T.P. Barnett and K.E. Kenyon, "Recent advances in the study of wind waves," Rep. Prog. Phys., 38, 1975, 667-729.

10. H. Mitsuyasu, "Measurement of the high-frequency spectrum of ocean surface waves," J. Phys. Ocean., 7, 1977, 882-891.

11. S.A. Kitaigorodskii, "The statistical characteristics of wind-generated short gravity waves," in Spaceborne Synthetic Aperture Radar for Oceanography, R.C. Beal, et al, eds., The Johns Hopkins University Press, 1981.

12. C.S. Cote, et al, Meteorological Papers, 2(6), W.J. Pierson, Jr., ed., 1960.

13. M.S. Longuet-Higgins, D.E. Cartwright, and N.D. Smith, Ocean Wave Spectra, Prentice-Hall, 1963, 111-136.

14. D.E. Cartwright and N.D. Smith, Buoy Technology, Marine Technology Society, Washington, D.C., 1964, 112-121.

15. J.A. Ewing, J. Marine Res., 27, 1969, 163-171.

16. O.M. Phillips, "The structure of short gravity waves on the ocean surface," in Spaceborne Synthetic Aperture Radar for Oceanography, R.C. Beal, et al, eds., The Johns Hopkins University Press, 1981.

17. B.A. Hughes, "The effect of internal waves on surface wind waves. 2: Theoretical analysis," J. Geophys. Res., 83, 1978, 455-465.

18. H. Hasselmann, Basic Developments in Fluid Dynamics, Vol. 2, M. Holt, ed., Academic Press, 1968, 117-182.

19. M.S. Longuet-Higgins, "On the nonlinear transfer of energy in the peak of a gravity-wave spectrum: a simplified model," Proc. Roy. Soc., A, 437, 1976, 311-328.

20. T.P. Barnett, "On the generation, description, and prediction of ocean wind waves," Ph.D. dissertation, University of California, San Diego, 1966.

21. T.P. Barnett, "On the generation, description, and prediction of ocean wind waves," J. Geophys. Res., 73, 1968, 513-529.

22. J.A. Ewing, "A numerical wave prediction for the North Atlantic Ocean," Deutsche Hydrog. Z., 24, 1971, 241-261.

23. O.M. Phillips, "On the interactions between internal and surface waves," Phys. Atmos. and Oceans, 9, 1973, 954-961.

24. J.E. Lewis, B.M. Lake, and D.R.S. Ko, "On the interaction of internal waves and surface gravity waves," J. Fluid Mech., 63(4), 1974, 773-800.

25. C. Garrett and J. Smith, "On the interaction between long and short surface waves," J. Phys. Oceanogr., 6, 1976, 925-930.

26. O.M. Phillips, "The dispersion of short wavelets in the presence of a dominant long wave," J. Fluid Mech., 107, 1981, 465-485.

27. O.H. Shemdin, "Modulation of centimetric waves by long gravity waves: Progress report on field and laboratory results," NATO Conference on Turbulent Fluxes Through the Sea Surface, Wave Dynamics and Prediction, A. Farve and K. Hasselmann, eds., NATO Conference Series V, vol. 1.

28. E.D. Graves and O.H. Shemdin, "An investigation of the modulation of capillary and short gravity waves in the open ocean," J. Geophys. Res., 85(C9), 1980, 5019-5024.

29. G.R. Valenzuela and J.W. Wright, "Modulation of short gravity-capillary waves by longer-scale periodic flows--a higher-order theory," Radio Science, 14(6), 1979, 1099-1110.

30. M.J.H. Fox, "On the nonlinear transfer of energy in the peak of a gravity-wave spectrum--I," Proc. Roy. Soc., A 348, 1976, 467-483.

31. K. Hasselmann, et al, "Measurements of wind wave growth and swell decay during the Joint North Sea Wave Project (JONSWAP)," Herausgegeben von Deutsche Hydrograph. Institut, Reihe A, 12, 1973.

32. D. Holliday, "Nonlinear gravity-capillary surface waves in a slowly varying current," J. Fluid Mech., 57(4), 1973, 797-802.

33. M.S. Longuet-Higgins, "The instabilities of gravity waves of finite amplitude in deep water, Part I: Superharmonics," Proc. Roy. Soc. A 360, 1978, 471-488.

34. R.C. Beal, "Spaceborne imaging radar: monitoring of ocean waves," Science, 208, 1980, 1373-1375.

35. D.D. Evans and D.H. Shemdin, "An investigation of the modulation of capillary and short gravity waves in the open ocean," J. Geophys. Res., 85, 1980, 5019-5024.

36. H. Mitsuyasu, "Interactions between water waves and wind (I)," Rep. Res. Appl. Mech., Kyushu University, 14, 1966, 67-88.

37. O.M. Phillips and M.L. Banner, "Wave breaking in the presence of wind drift and swell," J. Fluid Mech., 66, 1974, 625-640.

38. A.E. Gargett and B.A. Hughes, "On the interaction of surface and internal waves," J. Fluid Mech., 52(1), 1972, 179-191.

39. B.A. Hughes and H.L. Grant, "The effect of internal waves on surface wind waves. 1: Experimental measurements," J. Geophys. Res., 83, 1978, 443-454.

40. L.M. Brekhovskikh, et al, "On the resonant generation of internal waves through nonlinear interactions of surface waves," Bull. (Dzv.) Acad. Sci. USSR, Atmos. and Oceanic Phys., 8, 1972, 192.

41. R.C. Beal, "Introduction," Spaceborne Synthetic Aperture Radar for Oceanography, R.C. Beal, et al, eds., Johns Hopkins University Press, 1981.

42. R.O. Hagar, "SAR ocean imaging mechanics," in Spaceborne Synthetic Aperture Radar for Oceanography, R.C. Beal, et al, eds., Johns Hopkins University Press, 1981.

43. G.R. Valenzuela, "An asymptotic formulation of SAR images of the dynamical ocean surfaces," Radio Science, 15(1), 1980, 105-115.

44. W.R. Alpers, D.B. Ross, and C.L. Rufenach, "On the detectability of ocean surface waves by real and synthetic aperture radar," J. Geophys. Res., 86(C7), 1981, 6481-6498.

APPENDIX: IMAGING FOR REMOTE RADAR SENSING

Beal (Ref 41) discusses the fundamentals of aperture synthesis for the Seasat SAR (synthetic aperture radar). More detailed discussions of imaging for remote radar sensing are found in Ref 42-44. Seasat SAR obtains its high resolution by artificially synthesizing an aperture many kilometers long in space. For studying the ocean, SAR has two essential advantages over other high-resolution remote sensors: it collects its data through cloud cover and without help from the sun. It has demonstrated the potential ability to image and globally monitor ocean wave systems. SAR is sensitive primarily to the structure of the short gravity waves (30-cm waves for Seasat SAR) on the ocean surface that were shown in Section III to be sensitive to wind velocity, surface currents, swell, and internal waves.

According to classical diffraction theory, the angular resolution of any transmitting or receiving system, including SAR, is ultimately limited by the size of its aperture. Expressed simply

$$\phi = 1/\ell \ , \qquad \text{(A-1)}$$

---

41. R.C. Beal, "Introduction," Spaceborne Synthetic Aperture Radar for Oceanography, R.C. Beal, et al, eds., Johns Hopkins University Press, 1981.

42. R.O. Hagar, "SAR ocean imaging mechanics," in Spaceborne Synthetic Aperture Radar for Oceanography, R.C. Beal, et al, eds., Johns Hopkins University Press, 1981.

43. G.R. Valenzuela, "An asymptotic formulation of SAR images of the dynamical ocean surfaces," Radio Science, 15(1), 1980, 105-115.

44. W.R. Alpers, D.B. Ross, and C.L. Rufenach, "On the detectability of ocean surface waves by real and synthetic aperture radar," J. Geophys. Res., 86(C7), 1981, 6481-6498.

where ϕ is the angular resolution and ℓ is the size of the aperture expressed in wavelengths. When the same aperture is used for both the transmitter and the receiver of energy, as it is in SAR, the resulting angular resolution ϕ' is effectively halved (ie, $\phi' = \phi/2$). The Seasat orbited at a slant range h (20° from its nadir) of about 10^6 m and contained a SAR that operated at a radar wavelength of 0.2 m. The length L of the synthetic aperture is related to the azimuth resolution r_a (the ground resolution in the flight direction of the satellite) by

$$r_a = \phi' h = \frac{\lambda}{2L} h \ . \qquad \text{(A-2)}$$

An azimuth resolution of 25 m requires a synthetic aperture of 4 km. A satellite traveling at an altitude of about 10^6 m has an orbital velocity of about 8 km/s and, therefore, requires about 0.5 s to synthesize the required aperture.

Note that the length of the real aperture D on the spacecraft has not explicitly entered into the equations. However, the real aperture must be short enough to allow a particular point on the ground to remain entirely within the real beam $\theta = \lambda/D$ during the aperture synthesis interval. This leads to the relationship

$$L = h\frac{\lambda}{D} \ . \qquad \text{(A-3}$$

Combining Eq (A-2) and (A-3) leads to the fundamental lower limit for resolution

$$r_a = D/2 \ . \qquad \text{(A-4)}$$

Therefore, if a ground resolution of 25 m is desired, the real aperture can be no longer than 50 m to maintain a point in the real beam for a sufficiently long time. The resolution limit is independent of range because the time during which a particular point is illuminated increases with range, thus allowing a corresponding larger synthetic aperture to be formed. The Seasat SAR has a real aperture length of about 12 m and was, therefore, theoretically capable of an azimuth resolution of 6 m. This assumes that the maximum allowable synthetic aperture of 16 km could be constructed, a distance that is covered by the satellite in about 2 s.

Although a resolution of 6 m in azimuth is theoretically possible from Seasat, the imagery is typically processed to yield only 25 m. That is, only 4 km of synthetic aperture (about 0.5 s of data) are simultaneously processed. Any 4 m from the total 16 km length will satisfactorily produce a resolution of 25 m. Moreover, since the predominant system noise in the SAR is caused by "coherent speckle," which tends to be Rayleigh distributed in amplitude (ie, there are wide variations in the reflected signal from a resolution element as the illumination angle is slightly varied), each 4-km segment potentially allows an independent sample of the "average" reflectivity distribution. Therefore, the variance within a scene can be reduced considerably by separately processing and combining four independent 25-m images.

Thus far the discussion has dealt only with the very basic criteria for obtaining high azimuth resolution along the velocity vector of the satellite. We have not examined the actual mechanics of collecting and processing the information to reform the image, nor have we expanded our discussion to include the orthogonal (range) dimension. It should be apparent, however, that the synthetic aperture must be constructed with extreme care to realize its potential fully. For example, the azimuth resolution suffers if the

satellite is perturbed from the perfect trajectory by a significant fraction of its operating wavelength (23 cm for Seasat) as it traces out the 16-km aperture. Various types of aberrations can occur, all of which lead ultimately to loss of resolution and contrast in the image.

Having explored some of the fundamental requirements for aperture synthesis, we shall now summarize systematically the major steps in forming an image in terms of a stationary point-source response. Because an imaging system must be essentially linear, superposition arguments can extend the results to an arbitrary distribution of radar backscatter. A point source (step 1) having been illuminated by a coherent radar, emits a series of concentric wavefronts (step 2). Of course, the emission occurs only while the point source is within the aperture beam, as discussed above. The spacecraft cuts through the concentric wavefronts (step 3) and the SAR receiver intercepts an energy flux that varies with position (or time) as the wavefronts are traversed (step 4). This wavefront record is usually referred to as the Doppler—or signal—history, but it can also be considered a hologram, diffraction pattern, or a one-dimensional zone plate. The essential point is that this wavefront record, which contains a complete phase and amplitude history of the point source for the entire synthetic aperture interval, also contains adequate information to reproduce a diffraction-limited version of the original point source. The wavefront record is transferred via a data link (step 5) from the spacecraft to any of several ground stations, where it is recorded on either digital tape or optical film. For Seasat, the signal was normally recorded on tape at the station and was later transferred to film at a central facility. To reproduce the point source from the wavefront record, a coherent reference function (such as a family of plane waves from a laser) (step 6) impinges on the

Doppler history (step 7). The Doppler history, which is essentially the diffraction pattern of a point source, causes a lens-free convergence of the plane waves in free space (step 8) and forms a replica of the original point source.

In practice, there are several variations to the simple scheme described above, some of which are helpful, some nuisances, and others inevitably destructive. A simple lens inserted at step 8 can shorten the convergence distance. On the other hand, the spacecraft trajectory (step 3) is better described by an arc of varying center of curvature than by a straight line. This is clearly a nuisance, entailing an adaptive processing strategy. Atmospheric turbulence, reference function instabilities, and lens aberrations are examples of destructive and uncorrectable sources of contamination. Much of the effort and expense of spaceborne SAR can be attributed to the need to account precisely for the systemic sources of contamination and to minimize the random sources.

The extension of SAR image formation to the range (cross-velocity) direction is straightforward, but it places strict timing and synchronization requirements on the design and severely restricts the total range interval (or corresponding ground swath width) that can be accommodated. Range information is possible in a SAR only because the synthetic aperture need not be continuous, but may be constructed with samples; that is, the transmitter may be pulsed. It is enough that one pulse be transmitted each time the real aperture moves by half its length. This is called "filling the aperture" and leads to a maximum time interval τ of $D/2v$, during which range information can be collected. For $D = 12$ m and $v = 8$ km/s, $\tau = 750$ μs. In actual practice, the aperture is slightly "overfilled" to reduce the possibility of spurious signals that could lower image contrast. The Seasat SAR, for example,

typically operated at an interpulse period of 600 μs. Moreover, somewhat less than half of this time interval represented signals of sufficient quality to produce good imagery.

The synchronization constraints imposed by the Seasat geometry were as follows. Transmitter pulses are emitted every 600 μs in the cross-track direction, 20° away from nadir. The pulses form concentric expanding rings of energy with a separation of about 200 km ($c\tau = 3 \cdot 10^{8}$ m/s $\times$ $600 \cdot 10^{-6}$ s $\simeq$ 200 km). With the satellite orbiting at an altitude of 800 km there are four such pulses descending at any time. Since the antenna illuminates only that region around 20° from nadir, no significant backscatter occurs except at a slant range of about 850 km. This is no accident, since the round-trip distance of 1700 km must be chosen to allow the return from a particular pulse to occur exactly between two subsequently transmitted pulses. The geometry and pulse interval for the Seasat SAR are chosen to allow the return from a given pulse to occur exactly midway between the eighth and ninth subsequent pulses. The middle 200 μs of return, τ_s, represents a swath width of about 100 km for the Seasat geometry. Large swaths inherently require long real apertures to adequately accommodate all ranges and simultaneously fill the synthetic aperture properly. This can be a serious limitation in spaceborne SAR.

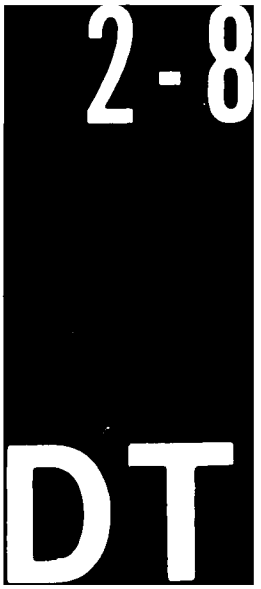
2-8
DT